Title
THE EROSION OF HEAT TREATED STEELS

Authors
Foley, T.
Levy, A.

Publication Date
1982-02-01

Lawrence Berkeley Laboratory
UNIVERSITY OF CALIFORNIA

Materials & Molecular Research Division

Submitted to Wear

THE EROSION OF HEAT TREATED STEELS

T. Foley and A. Levy

February 1982

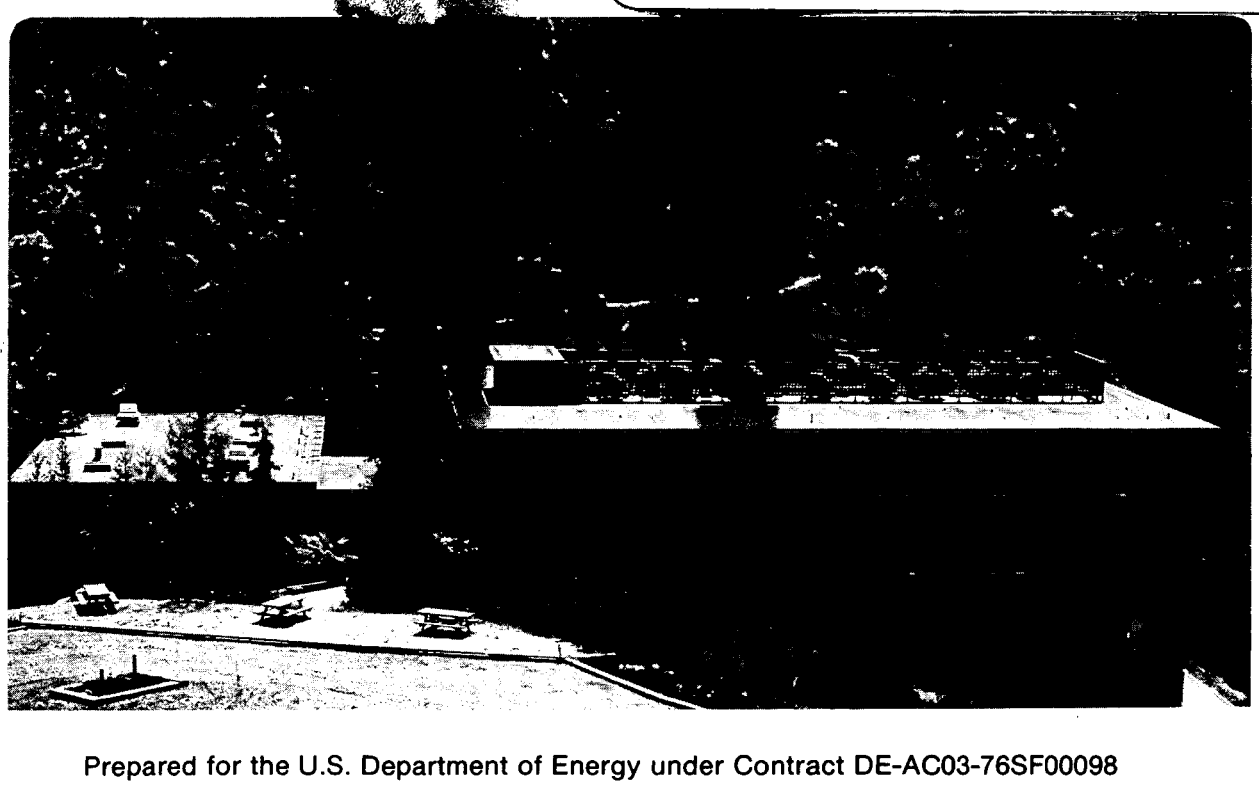

Prepared for the U.S. Department of Energy under Contract DE-AC03-76SF00098

DISCLAIMER

LBL-15241

THE EROSION OF HEAT TREATED STEELS

T. Foley and A. Levy

Materials and Molecular Research Division
Lawrence Berkeley Laboratory
University of California
Berkeley, California 94720

Research sponsored by the Department of Energy under DOE/FEAA 15 10 10 0, Advanced Research and Technical Development, Fossil Energy Materials Program, Work Breakdown Structure Element LBL-3.5 and under Contract No. DE-AC03-76SF00098.

ABSTRACT

The erosion behavior of a plain carbon steel (AISI 1020), an austenitic stainless steel (304), and a low alloy steel (AISI 4340) in various heat-treated conditions was determined. The testing was conducted at room temperature using 140μm average size aluminum oxide particles in an air stream. An attempt was made to characterize the erosion behavior as it relates to the mechanical properties obtainable in these alloys by conventional heat-treatments. It was determined that the ductility of the steels had a significant effect on their erosion resistance which increased with increasing ductility, and that hardness, strength, fracture toughness and impact strength had little effect on erosion behavior. The platelet mechanism of erosion occurred in all of the steels tested at all conditions.

INTRODUCTION

Solid particle erosion of components in coal conversion systems has been found to be a major problem in their development. This study was conducted in an attempt to contribute to the understanding of the mechanisms involved in erosion phenomena observed in ductile metals. In particular its objective is to understand the correlation between the erosion behavior of various steels and their mechanical properties as they are developed through heat treatments.

Several different mechanisms of erosion of ductile metals have been proposed through the years, beginning with a micro-machining process, and currently a mechanism of platelet formation and removal by a combined extrusion-forging process that takes place on the eroding surface [1, 2, 3, 4]. Some investigations have recently proposed a theory whereby the erosion is a result of the adhesion of the target material to the impacting particles[5]. However, evidence continues to build in support of the mechanism involving platelet formation and removal.

Most of the experimentation with ductile metals to this point has been conducted with aluminum and aluminum alloys. Very little information is available on steels. It is a secondary purpose here to try to ascertain whether or not the platelet formation mechanism of erosion can be considered as a general mechanism for ductile metals, or whether it might be peculiar to the aluminum alloys for which it was first defined.

EROSION, WEAR AND MECHANICAL PROPERTIES

Abrasive wear resistance has been shown by Kruschov to not be directly proportional to the hardness of metals (see Fig. 1) within a given family of steel alloys[6]. It is only directly proportional between different metallic elements. For example steel, being generally harder

and stronger than aluminum, shows better wear resistance. However, for a given family of steel alloys the wear resistance can actually increase with decreasing hardness. (See all alloys but 5 in Fig. 1). Fig. 2 illustrates this effect as observed in pure aluminum (1100-0) at a hardness of BHN 23 and a high strength aluminum alloy (7075-T6) at a hardness of BHN 150. This effect is only observed over a specific range of hardness because as the aluminum or steel becomes increasingly soft they reach a point where they have insufficient strength to resist the erosive force of the particle stream and the erosion resistance decreases again. This is illustrated for 1020 steel in Fig. 3 at three different levels of spheroidization. The spaces between carbide particles consists of soft, ductile ferrite.

This leads to the idea that the erosion behavior of a certain alloy may be more dependent upon properties such as ductility and toughness or rather the ability of a material to plastically deform without generation of fracture surface. Levy has discussed this at some length[7]. It is unfortunate, however, that properties such as ductility and toughness as they apply to the erosion mechanism where strain rates are very high are probably undeterminable. In order to determine the affect of the ductility on the erosion of a single phase alloy, 304SS was tested in the as-wrought and annealed conditions. 1020 steel was tested to determine how variations in the microstructure affected erosion behavior. Tests were conducted using AISI 4340 steel which was heat treated to a wide range of strength, hardness and toughness levels without as large a corresponding change in the tensile test elongation.

The effect of impingement angle on erosion behavior has been well documented in the past [1, 8]. Fig. 4 shows the impingement angle effect on a typical ductile and typical brittle material. Levy and Bellman discuss the various geometries of impact craters that are formed on the eroding surface of aluminum alloys at various

impingement angles and how this relates to their theory of platelet formation[2]. These crater geometries and platelet formations were observed on the steels tested in this program.

Velocity effects have also been investigated by numerous investigators. As might be expected intuitively, there is a strong dependence of erosion rate upon particle impact velocity due to the amount of kinetic energy imparted to the target material. There is still some disagreement as to just exactly how strong this dependence is and how it varies with erosion conditions. Finnie suggested that the amount of erosion damage suffered was proportional to approximately the square of the velocity[1]. He later modified this somewhat to velocity exponents of approximately 2.5 [9]. Laitone proposed velocity exponents up to four, considering the aerodynamic effects of particle flow on erosion [10]. Tabakoff calculated velocity exponents up to 5 based on erosion experiments performed in wind tunnel type testers[11]. Rickerby and MacMillan also predicted a greater dependence on velocity to match that measured in experiments[3].

An additional aspect that will be considered here is that of relating erosion behavior to the strain-hardening properties of a metal. Levy and Bellman suggested that a "steady-state" erosion condition is achieved after a subsurface zone of work-hardened material is established[2]. The strain hardening coefficient of the alloy being tested relates to the development of this zone.

This work substantiates recent claims concerning the effect of impingement angle, ductility, strength (hardness) and velocity on erosion rates and the proposed platelet formation mechanism of erosion of ductile metals. It generally refutes older claims for the effects of hardness and strength. it also proposes that additional variables are active in the erosion process than were considered in earlier investigations.

TEST DESCRIPTION

Test Conditions. All specimens were tested at room temperature in the erosion tester shown in Fig. 5. The carrier gas used was air. The eroding particles employed were 140μm (avg.) aluminum oxide of irregular shape, shown in Fig. 6. The distribution in particle size is given in Table I. The average particle load per test was 300 grams.

Table I

PARTICLE SIZE DISTRIBUTION*

Particle Size Range	% of Particle Sample in Range
>177μm	neg.
149 - 176	14.6
126 - 148	46.0
106 - 125	26.0
<105	13.4

*Avg. particle size = 140μm

Particle velocities were obtained by varying the pressure drop across the exit nozzle of the tester and were measured by the double-rotating disk method. A computer program has been developed for relating pressure drop and velocity for one dimensional flow that generally gives good results[12]. Tests were conducted at particle velocities of 30, 60 and 90mps (100, 200 and 300 ft/sec [approx.]). Very precise measurments of particle velocities in the immediate vicinity of the impact with the specimen are hard to achieve due to aerodynamic effects and rebound phenomena in the gas/particle stream at the stream/specimen interface. Laitone has discussed these factors at some length [10, 13].

Tests were conducted at particle impingement angles of 30° and 90°. The minimum resistance of ductile metals to solid particle erosion occurs at impingement angles in the range of 20° - 30° and for brittle materials it is at 90° or near-normal impact (see Fig. 4). Because of the aforementioned aerodynamic effects and other reasons,

the actual impingement angles for individual particles cannot be measured. Rather, the angle between the direction of the main particle stream from the nozzle and the specimen surface is reported.

The erosion measured in each test is generally plotted as weight loss or weight loss/gm of particles against the amount of impacted particles, in an incremental manner. That is, the amount of erosion weight loss for each increment of particles, i.e., 30gm or 60gm, etc., is plotted. This involves using an incremental weight loss measurement for each blast of particles where the weight of the specimen after the last blast is substracted from the weight at the beginning of the blast. Thus, the efficiency of each increment of particles in eroding the specimen is presented and the steady state condition at which each increment of particles removes the same amount of target material can be observed.

Specimen Preparation. 1020 steel in approximately 3mm (0.125") thick sheets was obtained in the hot-rolled condition. All specimens were austenitized at 950°C for one hour and water quenched. Some of the specimens were enclosed in argon-filled stainless steel bags and the carbides spheroidized for 10, 30 and 50 hours to obtain various degrees of spheroidized microstructures and levels of hardness and strength. All specimens were then polished to 600 grit, cleaned and weighed.

The 304 stainless steel sheet, 3mm thick, was obtained in the as-wrought condition. Half of the specimens were annealed at 1060°C for one hour and cooled in air. Specimen sections were thought to be thin enough to have a rapid enough cooling rate to insure that the carbides remained in solution. Test surfaces of these specimens were also polished to 600 grit.

The 4340 steel was obtained in 3mm thick sheet stock and subsequently austenitized and quenched in oil. Some of the specimens were

left as-quenched, some were tempered at 200°C ans some at 500°C for 1 hour to provide a high-toughness level, and some were spheroidized at 700°C for 30 hours.

The test surfaces of all of the 4340 specimens were ground to a RMS 16 or better finish prior to testing.

RESULTS

304 Stainless Steel. Stainless steel has a particular utility in erosion testing in that it is a common construction material for elevated temperature service and, hence, would be a likely candidate material for some components in coal-conversion systems where erosion can occur. Also, when annealed, 304SS has a measurable increase in its tensile percent elongation and reduction in area, two common measures of a material's ductility, without a corresponding decrease in strength

Fig. 7 shows that the as-wrought material at steady-state erosion has a 25% higher erosion rate than the annealed material at the same particle velocity and impingement angle. This is consistent with expected results because of the change in overall ductility as the result of annealing. The hardness of the material in the as-qrought condition was R_B 92, compared to values of approximately R_B 83 - 87 for the annealed material, not a significant difference. So, the erosion resistance of this alloy shows something of an improvement when annealed. However, it must be remembered that annealing of some stainless steels in the 300 series can sometimes have an adverse effect on their corrosion resistance. This is an additional consideration.

The 304SS also behaved as a conventional ductile metal in regards to impingement angle effect. Fig. 8 shows the effect of impingement angle, α, on the erosion behavior of the as-wrought material,

and Fig. 9 shows how the annealed material behaved. Note that the shapes of the curves are the same and that steady state erosion for both conditions occured around 60gms of erodent. Both conditions showed a two thirds increase in steady state erosion rate at α=30° compared to α=90°. This indicates that the basic erosion mechanism of 304SS is the same, only the rates differ. Also, the amount of particles required to reach steady-state erosion is approximately the same for both impingement angles, near 60gm of erodent.

Tests were also conducted at 3 velocities, 30, 60, and 90mps (100, 200, 300fps). As expected, there is a strong relationship between erosion and particle velocity. Fig. 10 and 11 illustrate this effect. The slope of the curve in Fig. 11 is near the 2.0 that relates to the kinetic energy of the particles (KE - 1/2 mv^2).

AISI 1020 Steel. The effect of microstructure on the erosion behavior of plain carbon steels has been determined on several occasions[14,15]. Levy obtained the results shown in Fig. 3 for 1020 steel in 3 carbide sizes of spheroidization[14]. In experiments at hand, however, the range of hardness achieved in the spheroidized steels was not as great and, consequently, the effect of increasing erosion rate at the greatest level of spheroidization achieved was not observed. A trend of increased erosion resistance was observed with decreasing hardness, and there seems to be a "leveling off" of this effect in the range of 30 - 50 Rockwell B-scale, R_B, hardness values. In Fig. 12 it is shown that for the first reduction of 20 points in hardness, there is a somewhat dramatic reduction in the observed steady state erosion rate. The next region of the curve, R_B 30 - 50, shows a very minor decrease in erosion rate with decreasing hardness that is insignificant. The actual minimum point, however, may occur at a significantly lower erosion rate than that shown in Fig. 12 at some hardness between R_B 30 and 50. Based on data from ref. 14, the erosion rate is expected to rise at lower hardness numbers, hence the dashed line portion of the curve (see Fig. 3).

The difference in absolute erosion rates in Fig. 3 and 12 is due to the different particle velocities used. The normal response to particle impingement angle was also observed in the spheroidized 1020 steel at the 3 levels tested and the curves for one spheroid size are shown in Fig. 13.

The difference in the erosion rates of hot and cold rolled 1020 steel are shown in Table II. The top portion of the table shows that cold rolled steel with a 15% elongation erodes considerably more than hot rolled steel which has a 25% elongation. This is yet another example of how the ability of the target metal to plastically deform under the impact of the eroding particles, thereby distributing the kinetic energy rather than having it concentrate to cause platelet fracture, directly relates to the erosion rate.

AISI 4340 Steel. 4340 steel was tested to determine how a martensitic steel behaves in a solid particle erosion environment at different heat treatments where major changes in the strength, ductility and toughness can be achieved. Table III shows the results of this test series. The erosion rates for specimens at all of the heat treat levels was nearly the same. This result is very similar to that obtained by Kruschov shown in Fig. 1, for abrasive type wear and by Gulden for erosion [6, 22]. The magnitude of the non-effect was large. The tensile strength and hardness variations of some 300% with little change in the erosion rates is significant. The adiabatic shear heating of the eroding surface is thought to remove the effects of any previous thermal treatment, thereby accounting for the lack of any effect of the heat treatment on the erosion rates.

The large increases in elongation and reduction of area in going from the as-quenched to the spheroidized heat treatment resulted in a relatively small decrease in erosion, of the order of 10%. It is felt that the basic ductility of the steel, especially at the high strain rates of the erosion process is in the same regime over the

TABLE 2

FFECT OF DUCTILITY,

STRENGTH, HARDNESS ON EROSION BEHAVIOR

OF 1020 CARBON STEEL

CONDITION	UTS	R_B	ELONG. %	EROSION WEIGHT LOSS[1]
HOT ROLLED	55KSI	65	25	2.8×10^{-3}g
COLD ROLLED	61KSI	70	15	4.0×10^{-3}g

HR 1020 STEEL DBTT TEST TEMPERATURE[3]	ELONG. %	EROSION WEIGHT LOSS[2]
25°C	25	2.5×10^{-3}g
-75°C	1-5	8.3×10^{-3}g

1. STATISTICAL AVERAGE OF INCREMENTAL WEIGHT LOSS PER 30gm LOAD OF 140μm Al_2O_3 PARTICLES AT STEADY STATE EROSION $\alpha = 30°$ V = 30mps T = 25°C

2. STATISTICAL AVERAGE OF INCREMENTAL WEIGHT LOSS PER 30gm LOAD OF 140μm Al_2O_3 PARTICLES AT STEADY STATE EROSION $\alpha = 90°$ V = 30mps T = 25°C

3. DUCTILE - BRITTLE TRANSISTION TEMPERATURE (DBTT) = -18°C

TABLE 3

EFFECT OF DUCTILITY,

STRENGTH, HARDNESS ON EROSION BEHAVIOR

OF 4340 STEEL

HEAT TREAT CONDITION	UTS	R_C	ELONG.%	RED IN AREA (%)	k_{1_c} KSI-In½	CHARPY IMPACT (Ft. lbs.)	EROSION WEIGHT LOSS*
AS-QUENCHED	307KSI	60	8	24	34	10	1.03MG
200°C TEMP.	273	53	11	36	58	16	0.97
500°C TEMP.	182	39	14	47	62	12	0.97
SPHEROIDIZED ANNEAL	~100	~19	~25				0.90

*STATISTICAL AVERAGE OF INCREMENTAL WEIGHT LOSS PER 30GM LOAD OF 140μm Al_2O_3 PARTICLES AT STEADY STATE EROSION

$\alpha = 30°$

V = 30 mps

T = 25°C

range of heat treatments tested and is further equalized by the elevated temperatures at the eroding surface. Therefore, the decrease in erosion with increasing elongation would not be as dramatic as the absolute numbers would indicate.

The erosion behavior of the as-quenched steel supports the premise that all of the heat treat conditions of the 4340 steel tested are in a basically ductile regime. As can be seen in Fig. 14, the erosion at 30° impingement angle is much greater than at 90°, which is typical of ductile metals. The 200°C temper curve shown in Fig. 15 is similar, but has considerably less difference between the 30° and 90° angle erosion rates, only half of that which occurred in the as-quenched steel. This behavior indicates that as materials get more ductile, they are able to distribute the kinetic energy of the impacting particles in a less angle oriented manner.

The effect of toughness on the erosion of 4340 steel was less than expected, as can be seen in Table III. However, as for the elongation, the range of k_{1_c} appears to be in the same regime so far as erosion is concerned. The Charpy impact strength variation similarily, has no effect on the erosion of the 4340.

Effect of Strain Hardening. Levy and Bellman have proposed that a steady-state condition of erosion occurs when a sub-surface work-hardened zone which acts as an anvil is established in the target material[2]. This zone occurs beneath a softened, probably annealed surface zone caused by localized heating due to the severe plastic deformation of the surface material and possibly, surface friction between the particles and the erosion surface. The impacting particles act as hammers, extruding, then forging the hot, softened surface metal between them and the cold worked anvil into thin, highly distressed platelets. Hutchings discussed this in terms of the energy balance in particle impact[17]. Steady-state erosion of a ductile metal results when the condition of Fig. 16 is established. The

cross-sectional hardness distribution that would occur in such a model was varified by measuring the hardness distribution of the cross section of an eroded specimen. The micro-hardness test results for 1100-0 aluminum are shown in Fig. 17 [12].

There was concern about the validity of the hardness points obtained very near the surface due to a possible lack of support for the indentor. however, optical microscope analyses, Fig. 18, of these surfaces confirm the validity of points located from approximately 5μm below the surface down into the base metal. The symmetry of the indentations indicates that the indentor was evenly supported as it penetrated the metal. The first measurement plotted in Fig. 17 was the one 5μm in from the surface.

Fig. 19 is a plot of the micro-hardness readings on one of the 1020 steel specimens that was erosion tested in the study reported herein. The initial measurement shows very soft material about 4μm from the eroded surface. The next several readings are considerably higher than that of the bulk material, indicating the cold worked zone. At about 40μm from the surface, the hardness readings begin to fall within the range observed in the bulk material. Thus, both aluminium and steel show evidence of a soft, highly deformed surface area beneath which is a harder, sub-surface cold worked region that is above the bulk metal.

The establishment of the work hardened zone as a condition of steady-state erosion would imply that a material such as an austenitic stainless steel (e.g. 304SS), which has a strain hardening coefficient of 0.45 - 0.55 would achieve a steady-state erosion condition before a material such as 1020 carbon steel which has a strain hardening coefficient of 0.05 - 0.15. This is, in fact, observed. Comparison of the shapes of the curves in Fig. 20 shows that steady-state erosion is achieved when around 60 grams of particles impinged on the 304 stainless steel, while for the carbon steel it does not occur until more than 120 grams have struck the surface.

Fig. 20 also compares the amount of erosion between the mild steel and the 304SS, which are in a similar hardness and strength condition. The 304SS has a significantly lower erosion weight loss than does the 1020 steel. While the 304SS is somewhat harder and stronger than the 1020 steel, its primary difference is considerably greater ductility. It has approximately twice the elongation of the 1020 steel and 40% higher reduction of area, thereby accounting for its greater erosion resistance.

These results point away from hardness and strength as the major contributing factors to erosion behavior in ductile materials and toward consideration of properties such as ductility and malleability of metal as the principal properties that determine the ability of a ductile metal to withstand the effects of an erosive particle stream. The results of the 4340 steel tests appear to discount fracture toughness and Charpy impact strength effecting erosion behavior and give support to the idea that erosion behavior is strongly dependent upon the ductility or plastic deformation characteristics of the metals.

The number of particles required for the 4340 steel to reach steady-state erosion was independent of the heat treat condition. It can be seen in Fig. 14 and 15 that a steady state condition was reached in about 100gm of particles, the same number of grams of erodent as was required by the 1020 steel which has near the same strain hardening coefficient. The 500°C temper and spheroidized conditions also reached steady state erosion around 100gm of erodent. This indicates that it is the strain hardening coefficient of the metal rather than the specific heat treatment morphology or strength level that determines when steady-state erosion is reached.

Effect of Ductile-Brittle Transition Temperature (DBTT). In order to provide further verification of previous statements concerning the effect of ductility on erosion behavior of ductile metals, it was decided to conduct some tests above and below the ductile to brittle transition temperature (DBTT) of a steel, thereby achieving very

different levels of tensile ductility essentially without any microstructural changes. 1020 mild steel was selected for these tests, being basically ductile at 25°C with an elongation of 25% and much less ductile below its DBTT when mounted on a block of dry ice at approximately -78°C where its elongation was 1 - 5%.

After polishing, each specimen to be tested below the DBTT was secured to a 1" thick block of dry ice, installed in the erosion tester and subjected to a 150gm blast of aluminum oxide particles at 30mps (approx. 100fps). An equal number of erosion tests of 1020 steel from the same sheet were conducted at 25°C, which is above the -18°C DBTT of the hot rolled steel. All tests were at an impingement angle of 90°.

The average specimen weight loss in the low temperature test was 8.3×10^{-3}g. The specimens tested at 25°C lost only 2.5×10^{-3}g or less than one third of the loss that occurred below the DBTT where the ductility was only 20% of that at room temperature, as measured by tensile elongation. The test results are shown at the bottom of Table II. These tests provided further evidence that the greater the ductility of a ductile metal is, the greater its erosion resistance is.

Microstructure. Platelets, very similar to those observed on the eroded surface of 1100-0 Al, were evident for all materials tested in this study in all heat treated conditions[2]. Fig. 21 are SEM micrographs of the eroded surfaces of the 1020 steel for two impingement angles.

DISCUSSION

The erosion behavior of the steels investigated in this project further substantiated observations made in earlier studies at this laboratory regarding the mechanism of erosion and the direct relationship

between the ductility and the erosion resistance.[7, 14] As Kruschov reported for the case of abrasive wear 20 years ago, hardness and, hence, strength do not relate directly to wear resistance within regimes of alloys such as steels.[6] He observed that in major areas of the hardness spectra of steel alloys they can relate in an inverse manner, i.e., higher hardness and strength in alloys results in lower wear resistance.

The results of testing 3 different types of steel in the work reported herein showed the same types of relationships between hardness and wear/erosion resistance that Kruschov and Gulden found.[6, 22] The primary reason for ductility aiding erosion resistance is postulated to be the dissipation of the kinetic energy of the impacting particle by plastic deformation in the local region of the impact so that the local fracture stress of the platelets formed is not exceeded.

The use of heat treatments to effect differences in toughness and strength by modifying the microstructure of the alloys to affect their overall state of lattice strain hardening have minimal effects on erosion. The adiabatic shear and friction heating of the erosion surface removes the morphological and state of strain effects of the treatments in the immediate surface erosion region. It is the ductility of the bulk alloy that is the deterrent to erosion loss. Only when particles impacting an already highly plastically deformed area cause the local fracture stress of the distressed platelets to be exceeded can erosion loss occur. The effect of the very high strain rates that have been calculated to occur in erosion on the deformation and fracture behavior of alloys is not known.[20] However, reasonable correlations between erosion rates and slow strain rate tensile elongation can be made.

Reversal of the benefit of ductility enhancing erosion resistance has also been determined and is reported in this work. There

appears to be a limit of trading off lower strength for ductility to gain erosion resistance. If the local fracture strength of the alloy becomes lower than some limiting value, the force exerted by the impacting particle can exceed it. Fracture then occurs along with the plastic deformation, material is lost, and the erosion rate increases, even though the ductility of the alloy is still increasing.

Since the force imparted by the impacting particles directly relates to their velocity to an exponent greater than 2, at higher velocities than those used in this investigation it is expected that the impacting force would result in localized stresses that would exceed a higher fracture stress. In such a case the effect of ductility on erosion resistance would reverse itself at a lower ductility level. Thus, at higher velocities such as those that are encountered in the erosion of turbine blades, the ability of increased ductility to impart increased erosion resistance may be greatly reduced or even eliminated.

Depending on the alloy and the manner in which its strength and ductility levels were established, it is conceivable that the ductility effect observed in this work would not be observed. In work by Gulden and Kubrych on Fe-Cr binary single phase alloys, the conditions were such that strength and hardness directly related to erosion resistance[21]. These alloys were solid solution strengthened, unlike the tempered martensite strengthening of the 4340 steel. In this case, the localized plastic deformation upon particle impact was not sufficient to keep the resulting force from exceeding the fracture stress and only with higher fracture strengths was it possible to reduce the erosion rate. In that same investigation Gulden and Kubarych found that for 1095 steel greater ductility did result in greater erosion resistance. Thus, different alloys with different compositions and morphologies respond to erosion forces in opposite manners.

In this study the mechanism of erosion was always the same, regardless of the erosion rate that was measured. Platelets of metal were formed in the immediate surface region, were subsequently highly deformed by continuing particle impacts, and were eventually knocked off the surface when their local fracture stress was exceeded. Beneath the highly deformed surface region, a cold worked zone was developed that enhanced the ability of the impacting particles to form, deform and knock off platelets.

This mechanism of platelet formation and removal was initially observed and documented in this laboratory using aluminum alloys[2]. The fact that the same mechanism was observed on mild steel, austenitic stainless steel and a high strength alloy steel in several different microstructures in the work reported herein enhances the concept of the platelet mechanism of erosion.

CONCLUSIONS

1. The ductility of the steels tested, as measured by their tensile elongation, correlates most directly with erosion resistance. The greater the ductility, the greater the erosion resistance However, a limit to this relationship was determined.

2. Fracture toughness, Charpy impact strength, tensile strength and hardness of 4340 steel in the ranges tested in this investigation had little correlation with erosion behavior. Most, if not all, of the effect of the heat treatments used to modify these properties is mitigated by the adiabatic shear heating of the erosion surface that can cause the recrystallization temperature of the alloy to be reached.

3. The erosion mechanism of the steels tested in this investigation is the same as the platelet mechanism of erosion postulated by

testing aluminum alloys in earlier work. Micro-hardness traverses of steel specimens and other evidence verified this.

4. The time to reach steady-state erosion is a function of the strain hardening coefficient of the steel tested. The higher the strain hardening coefficient, the sooner steady-state erosion is reached. This correlates well with the need in the platelet mechanism of erosion to form a sub-surface cold worked zone before steady-state erosion occurs.

5. A longer spherodization time for 1020 steel with an accompaning decrease in hardness and increase in ductility resulted in less erosion occuring.

6. Annealing 304SS increases its erosion resistance over that of as -rolled steel. The difference is due to the increased ductility of the more erosion resistant form of the alloy.

7. Large strength and hardness differences in heat treated 4340 steel had, essentially, no effect on erosion rate.

8. The number of particles striking 4340 steel specimens to reach steady state erosion was independent of the heat treat level and appeared to primarily be related to the strain hardening behavior of the steel.

9. Erosion rates in steels increase markedly below the ductile-brittle transition temperature (DBTT) because of a major decrease in ductility.

This work is supported by the Technical Coordination staff of the Office of Fossil Energy of the U.S. Department of Energy under Contract Number DE-AC03-76SF00098 through the Fossil Energy Materials Program, Oak Ridge National Laboratory, Oak Ridge, TN.

REFERENCES

1. Finnie, I.; "The Mechanism of Erosion of Ductile Metals;" Proc. of the Third U.S. National Congress of Applied Mechanics; 1958

2. Bellman, R. Jr., Levy, A.; "Erosion Mechanism in Ductile Metals;" Wear 70 #1;pp 1-28; July, 1981

3. Rickerby, D.C., Macmillan, N.H.; "Erosion of Aluminum and Magnesium Oxide by Spherical Particles;" Proc. of the International Conference on the Wear of Materials; San Francisco, California; March, 1981

4. Brown, R., Jin Jun, E., Eddington, J.W.; "Mechanisms of Erosive Wear for 90° Impact on Copper and Iron Targets;" Proc. of the International Conference on the Wear of Materials; San Francisco, California; March, 1981

5. Salik, J., Buckley, D.H.; "Effect of Mechanical Surface and Heat-Treatments on Erosion Resistance;" Proc. of the International Conference on the Wear of Materials; San Francisco, California; March, 1981

6. Kruschov, M.M.; "The Correlations between Wear Resistance and Abrasive Wear and the Strength Properties of Metals;" Industrial Laboratory Vol 28, pp 372

7. Levy, A.V.; "The Role of Plasticity in Erosion;" Proc. of the Fifth International Conference on Erosion by Solid and Liquid Impact; Cambridge, United Kingdom; September, 1979

8. Finnie, I.; "An Experimental Study of Erosion;" Presented at the Spring Meeting of the Society for Experimental Stress Analyses; Washington, D.C.; 1959

9. Finnie, I., McFadden, D.H.; "On the Velocity Dependence of the Erosion of Ductile Metals by Solid Particles at Low Angles of Incidence;" Wear 48 #1;pp 181-190; 1978

10. Laitone, J.A.; "Aerodynamic Effects in the Erosion Process;" LBL report 8962; Lawrence Berkeley Laboratory, Berkeley, California; 1979

11. Tabakoff, W., Hamed, A., Ramaehandran, J.; "Study of Metals Erosion in High Temperatures Coal Gas Streams;" ASME, Engineering for Power, Vol 102, #1; January, 1980

12. Kleist, D.M.; "One-Dimensional - Two Phase Particle Flow;" (M.S. Thesis) LBL report 6967, Lawrence Berkeley Laboratory Berkeley, California; 1977

13. Laitone, J.A.; "Characterization of Particle Rebound Phenomina in the Erosion of Turbo-Machinery;" LBL report 1217; Lawrence Berkeley Laboratory, Berkeley, California; 1980

14. Levy, A.V.; "The Solid Particle Erosion Behavior of Steel as a function of Microstructure;" Wear 68, #3; pp 269-288; May, 1981

15. Jahanmir, S., Levy, A.V.; "The Effects of the Microstructure of Ductile Alloys on Solid Particle Erosion Behavior;" Proc. of the AIME Conference on the Corrosion-Erosion Behavior of Materials; St. Louis, Missouri; October, 1978

16. Ritchie, R.O.; "Further Considerations on the Inconsistency in Touchness Evaluation of AISI 4340 Steel Austenitized at Increasing Temperatures;" Met. Trans., 9A; March, 1978

17. Hutchings, I.M.; "Some Comments on the Theoretical Treatment of Erosive Particle Impacts;" Proc. Fifth International Conference on Erosion by Solid and Liquid Impact; Cambridge, United Kingdom; September, 1979

18. Levy, A.V; "Erosion of Elevated Temperature Corrosion Scales on Metals;" Wear, 73, #2; pp 355-370; November, 1981

19. Ritchie, R.O., Horn, R.M.; "Mechanisms of Tempered Martensite Embrittlement in Low-Alloy Steels;" Met. Trans. A., 9A, pp 1039; August, 1978

20. Hutchings, I.M.; "Strain Rate Effects in Microparticle Impact;" J. Physics, D: Applied Physics, 10, pp 151-156; 1977

21. Gulden, M.E., Kubarych, K.G.; "Erosion Mechanisms of Metals;" Report SR81-R-4526-02, Solar Turbines, Inc.; San Diego, California

22. Gulden, M.E.; "Influence of Brittle to Ductile Transition on Solid Particle Erosion Behavior;" Proc. of Fifth International Conference on Erosion by Liquid and Solid Impact"; Cambridge, United Kingdom; September, 1979

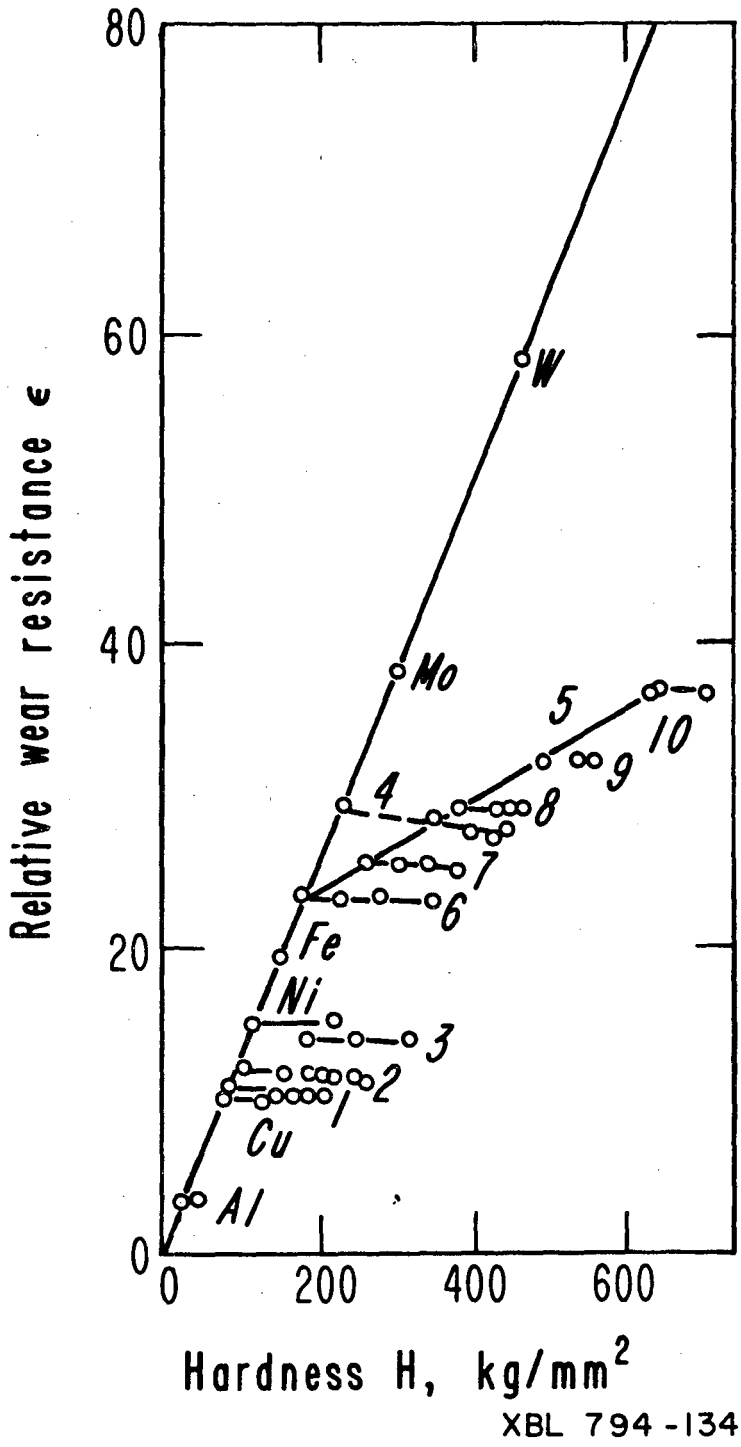

Fig. 1 Relative Wear Resistance ref. [6]

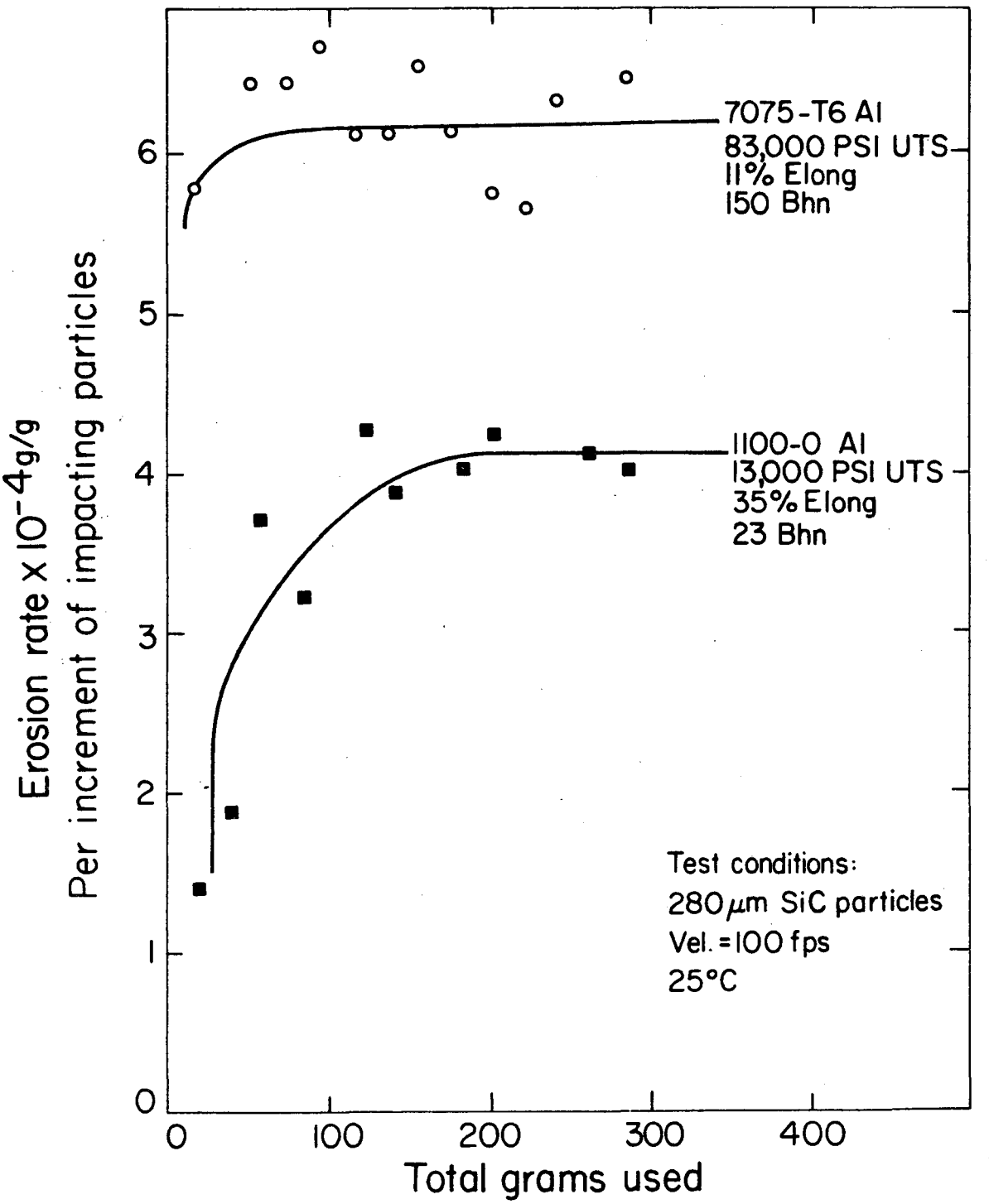

Fig. 2 Erosion Behavior of 1100-0 Aluminum and 7075-T6 Aluminum Alloy

XBL 8110-1379

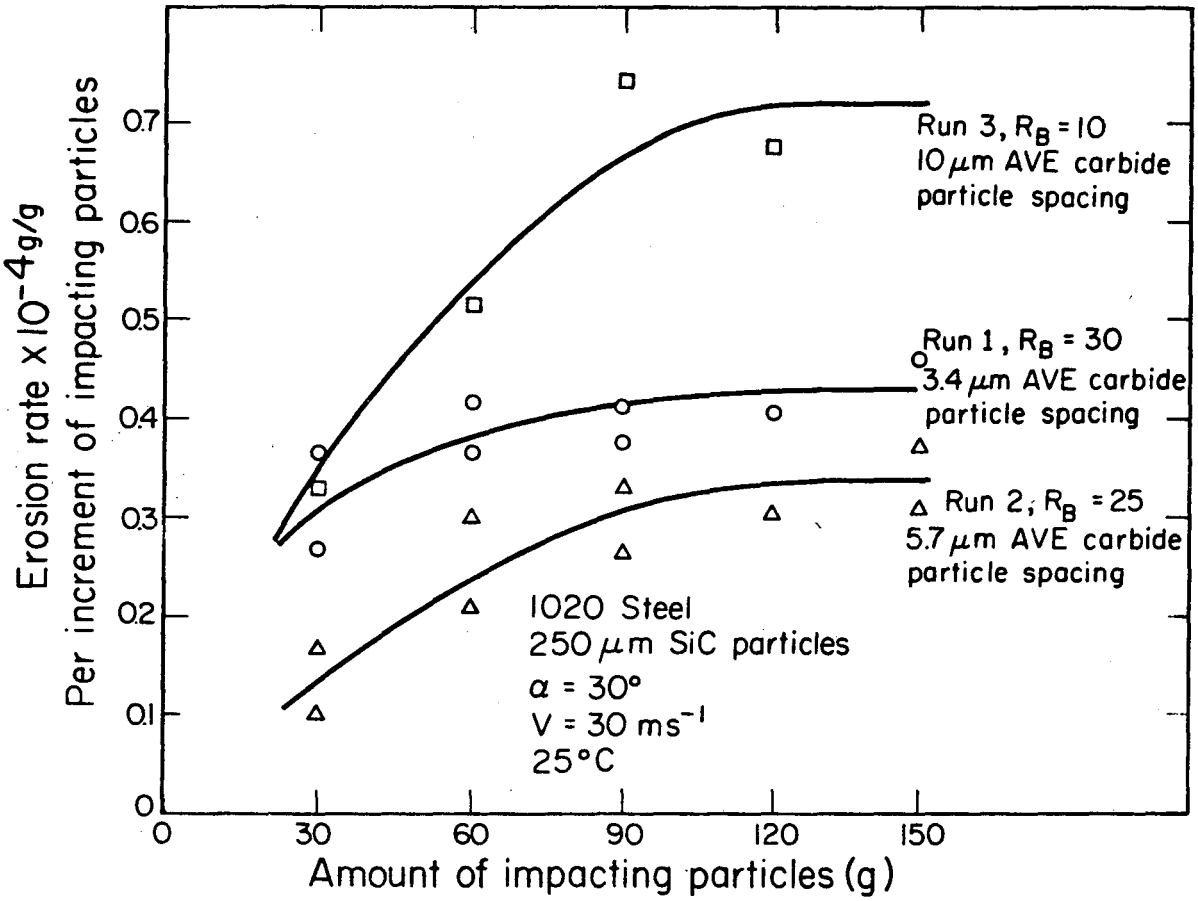

Fig. 3 Erosion rates of Spheroidized 1020 Steel at three different carbide sizes reg. [14]

XBL 804-700

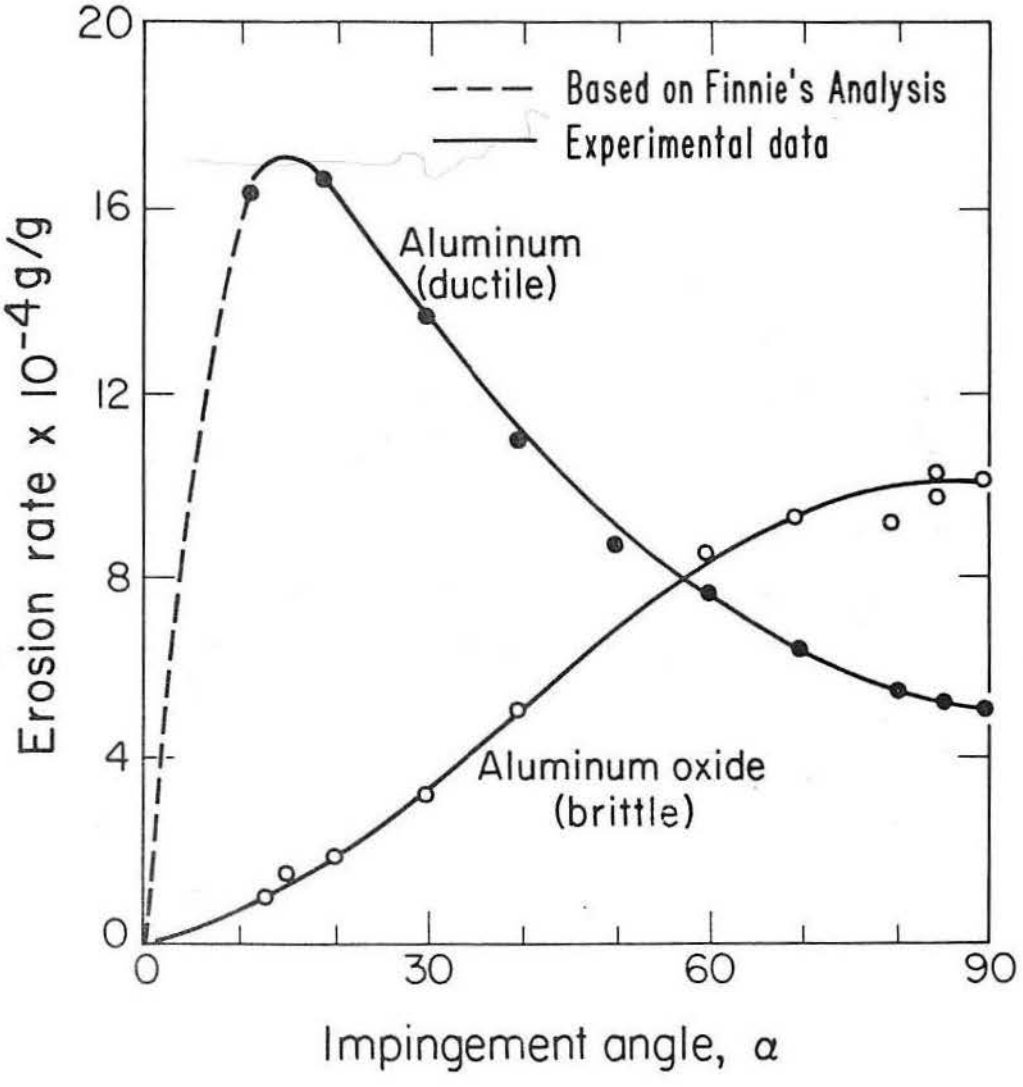

Fig. 4 Impingement Angle Effects on erosion of typically ductile and brittle materials ref. [1]

XBL 793-974

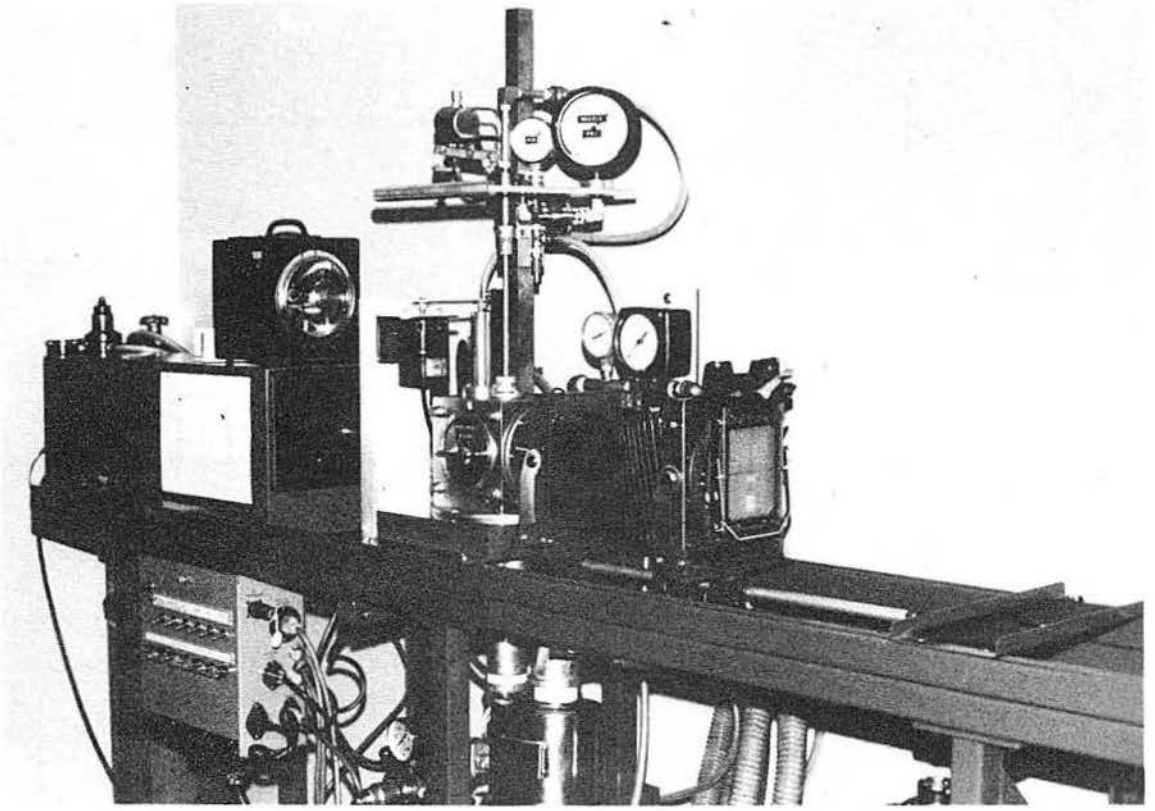

CBB 763-2073

Fig. 5 Room Temperature Erosion Tester

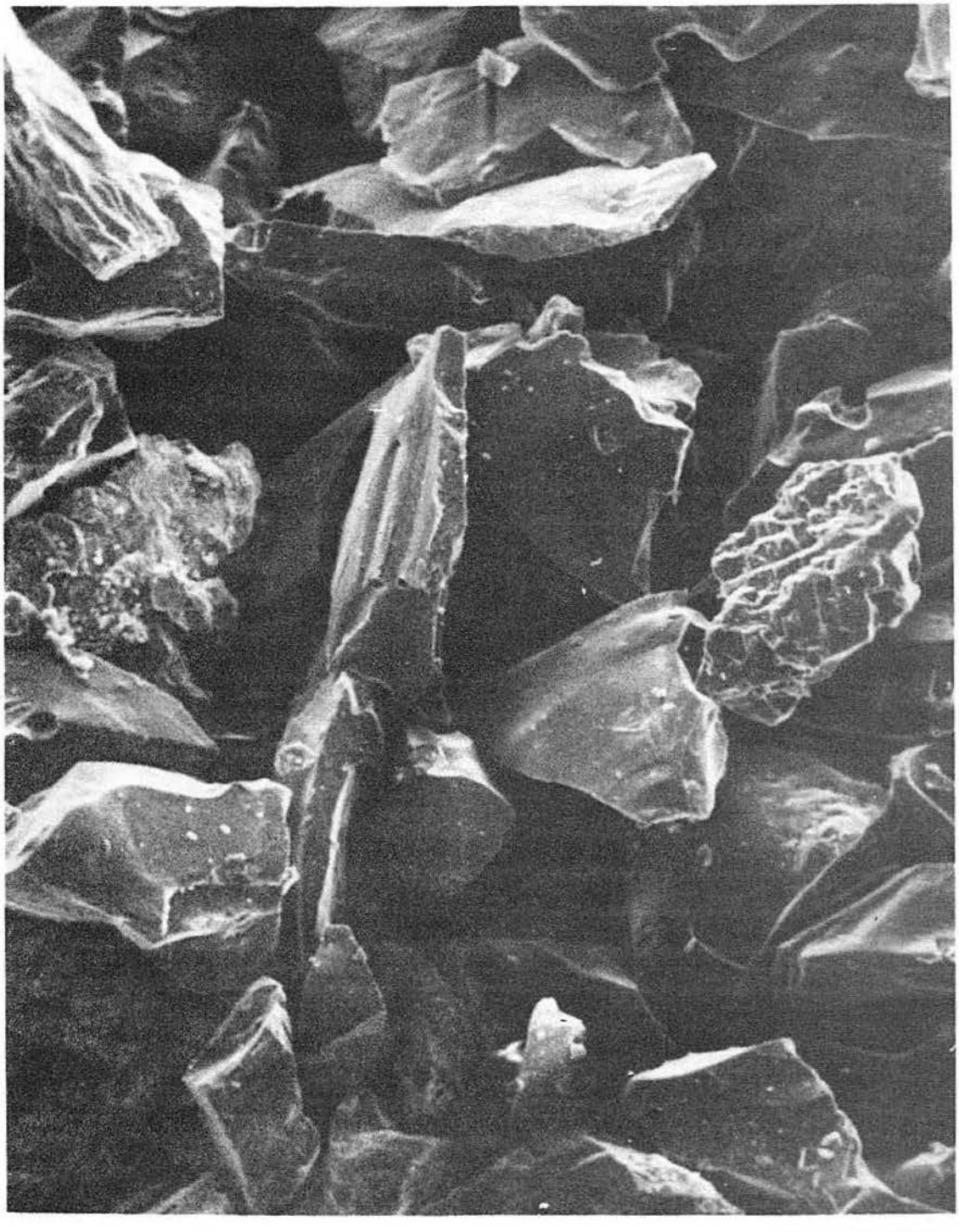

XBB 819-9063

Fig. 6 Al_2O_3 Particles

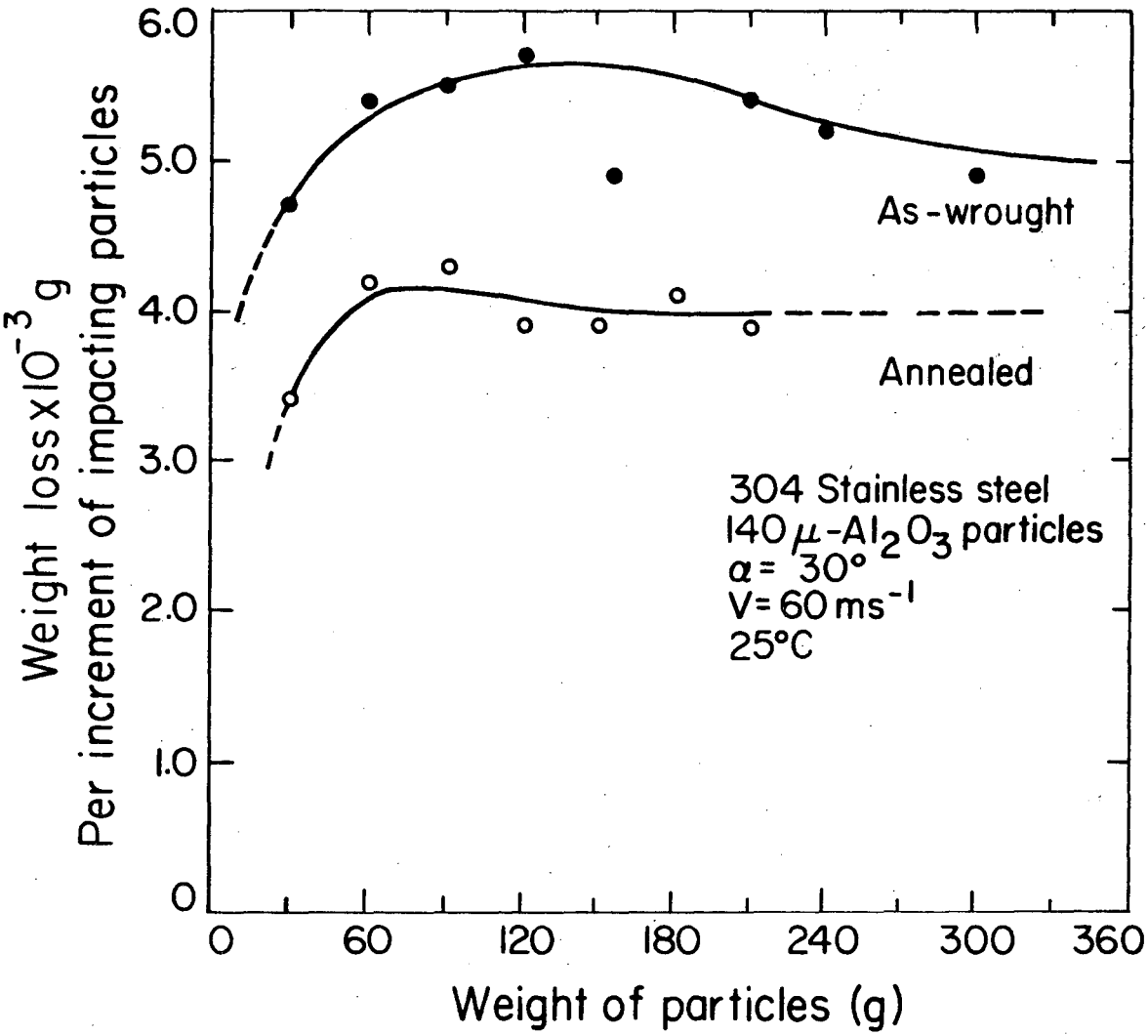

Fig. 7 Erosion of As-wrought and Annealed 304 SS

XBL 8110-1392

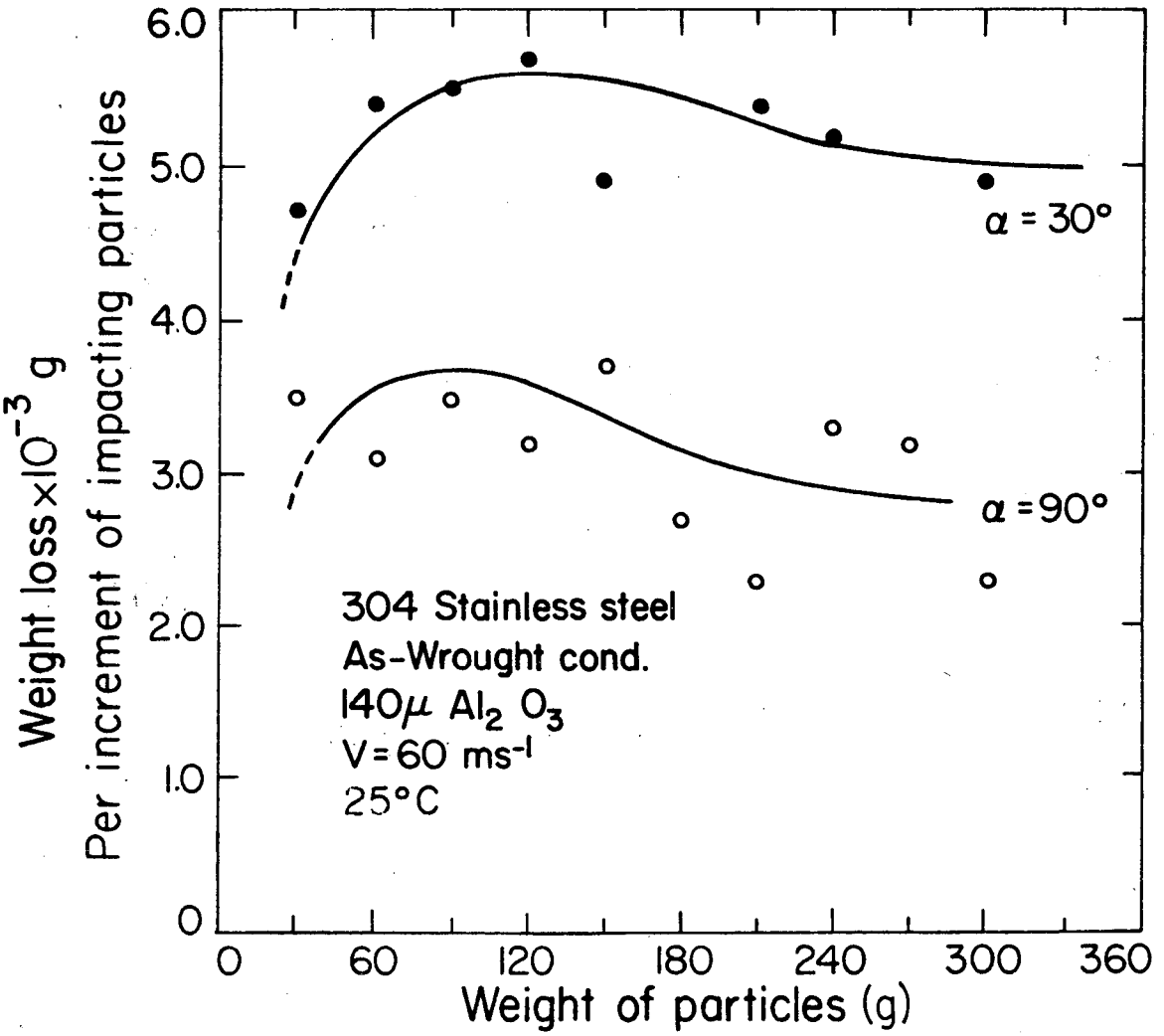

Fig. 8 Erosion of As-wrought 304 SS at α = 30° and 90° impingement angles

XBL 8110-1394

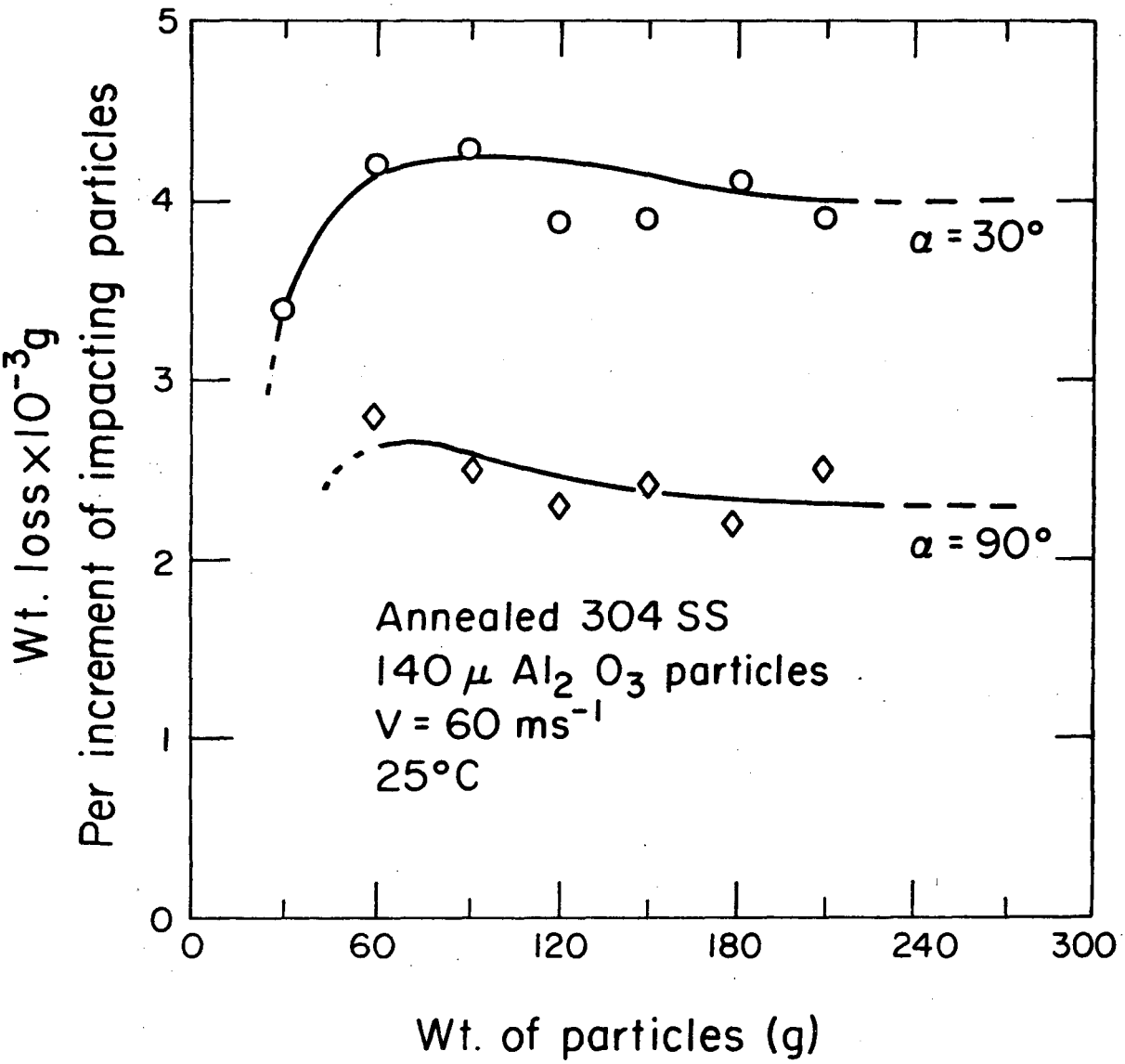

Fig. 9 Erosion of Annealed 304SS at α = 30° and 90° impingement angles

XBL 8111-12045

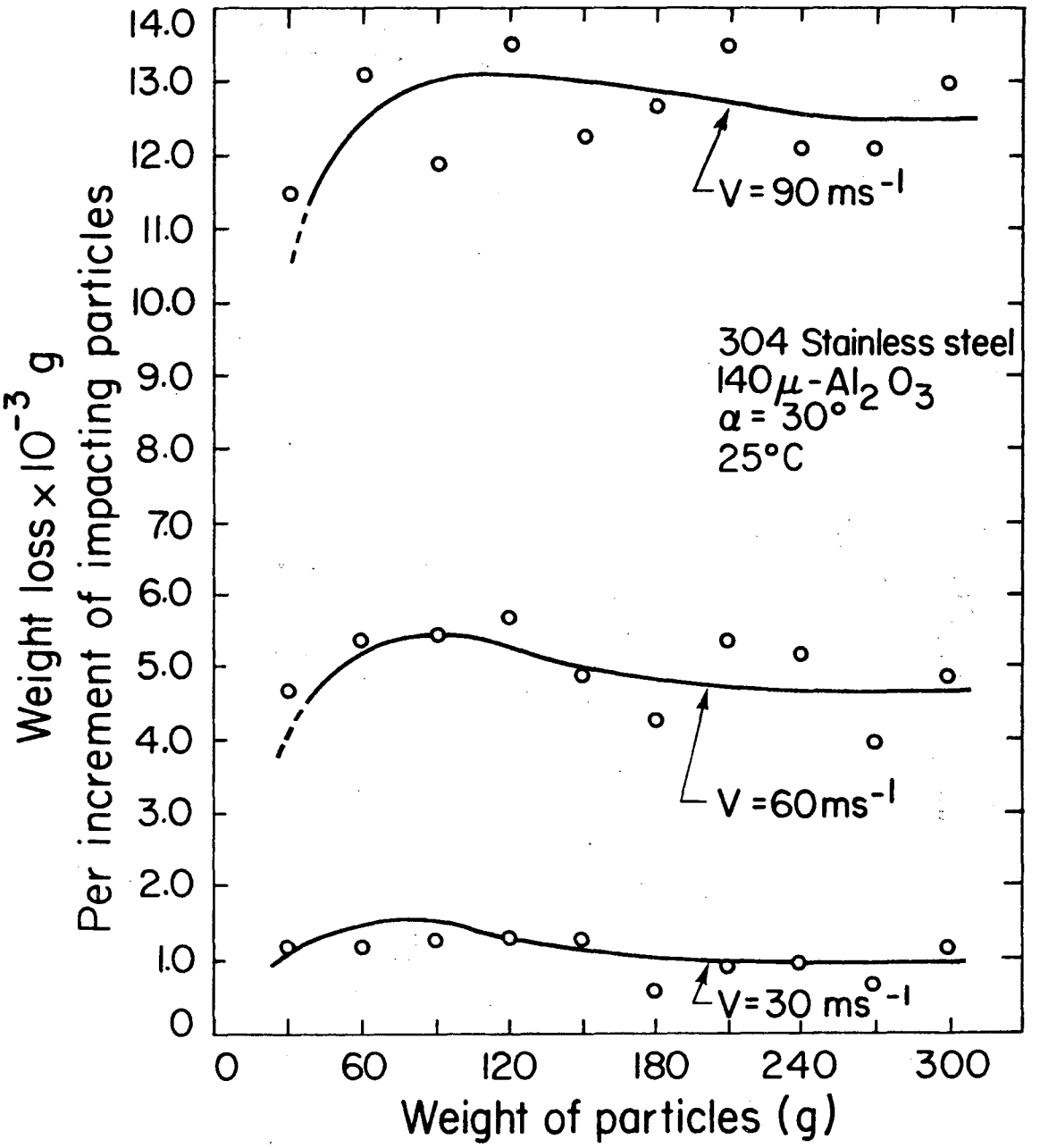

Fig. 10 Erosion of 304 SS at 30, 60, 90 mps

XBL 8110-1393

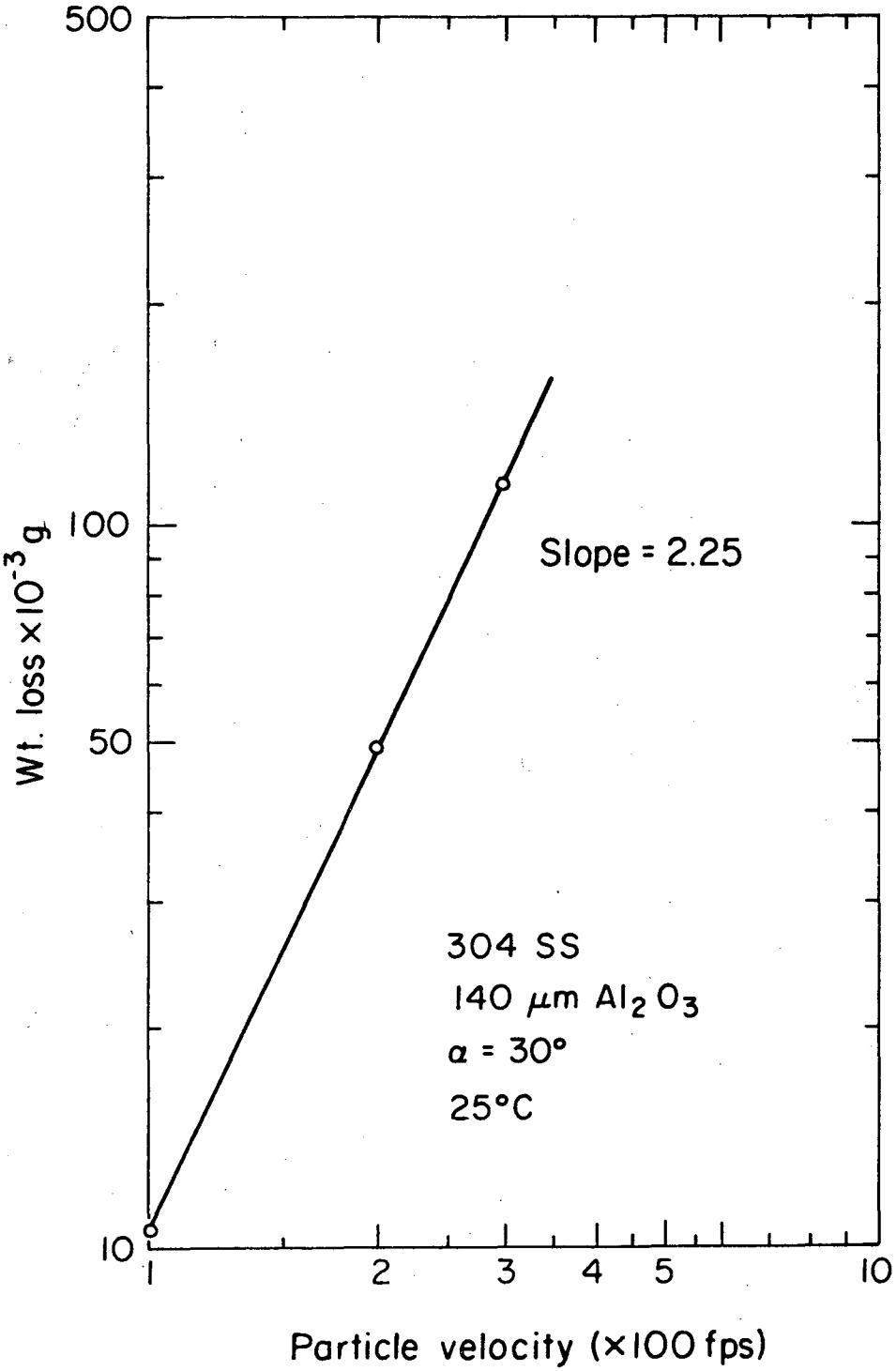

Fig. 11 Velocity Dependence in the Erosion of 304 SS

XBL8111-12040

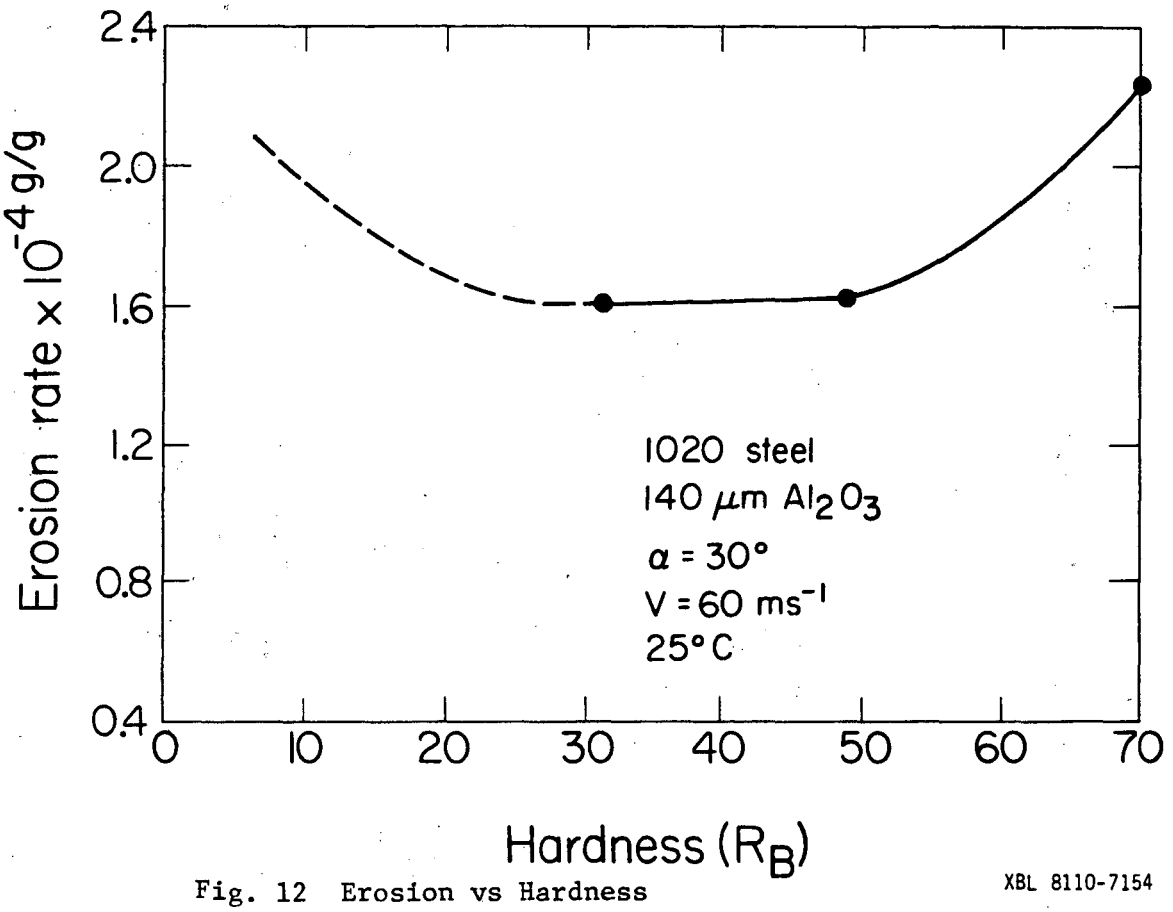

Fig. 12 Erosion vs Hardness for 1020 Steel

XBL 8110-7154

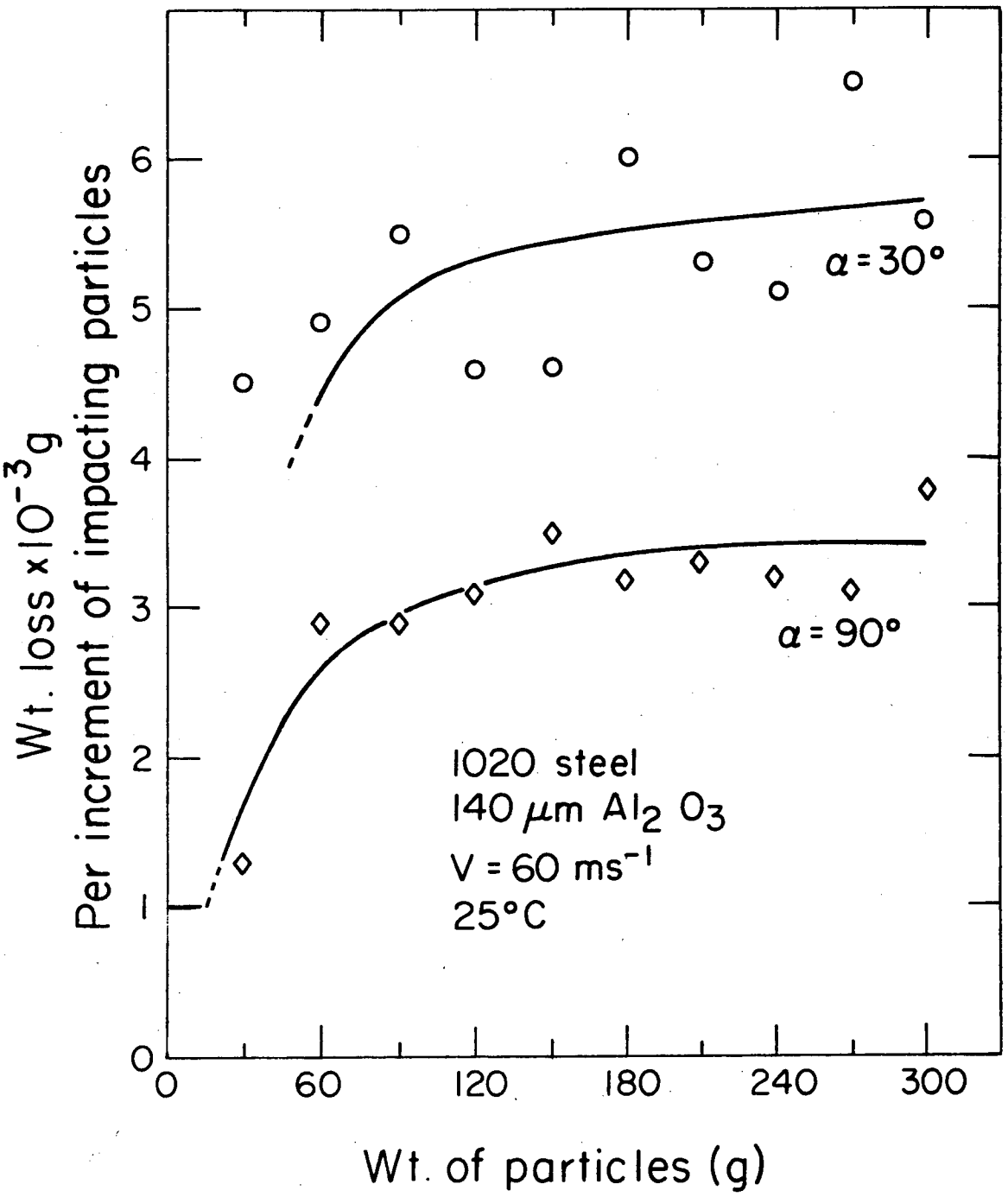

Fig. 13 Erosion of Spheroidized 1020 Steel at 30° and 90° impingement angles

XBL 8111-12044

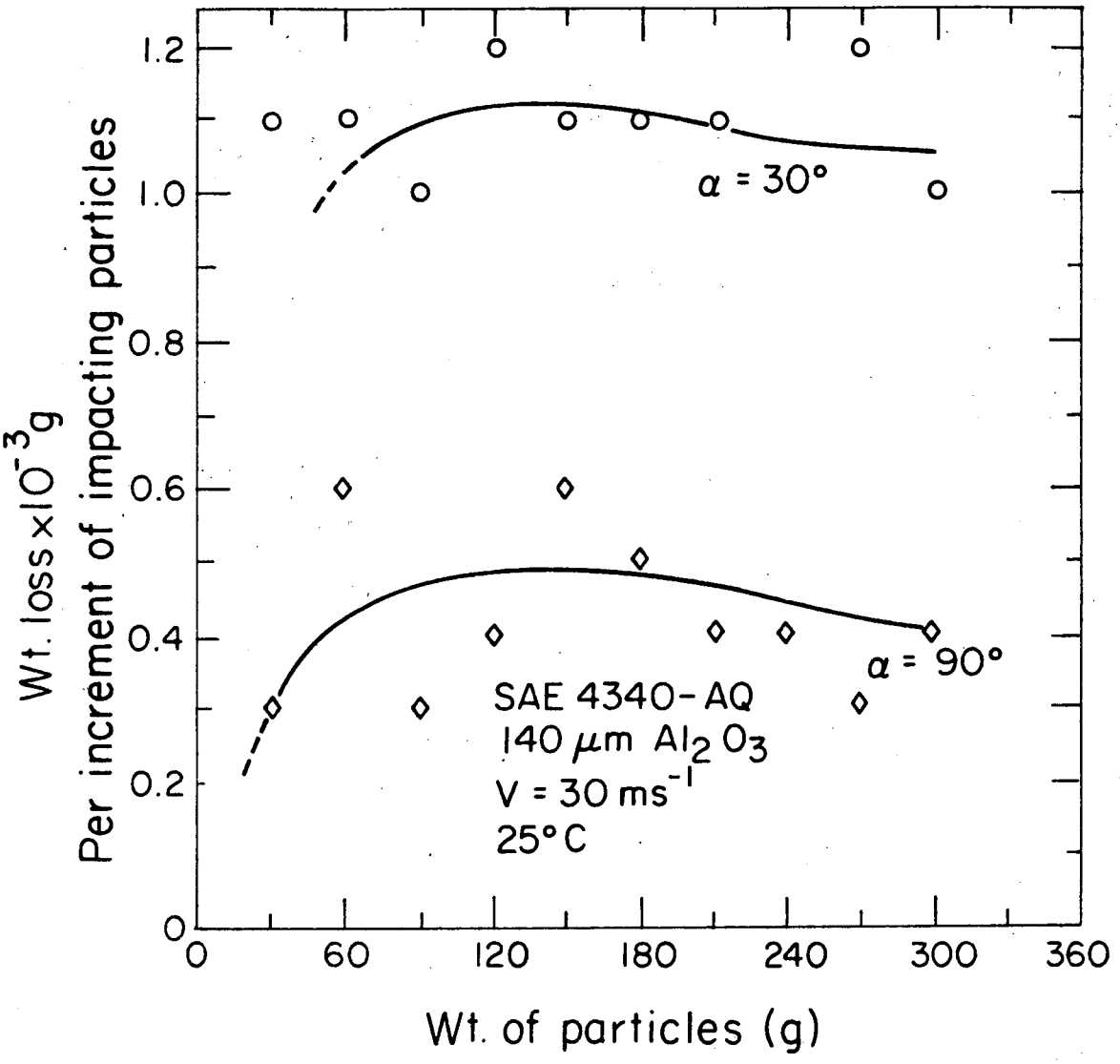

Fig. 14 Erosion of 4340 Steel As-Quenched Condition

XBL8111-12042

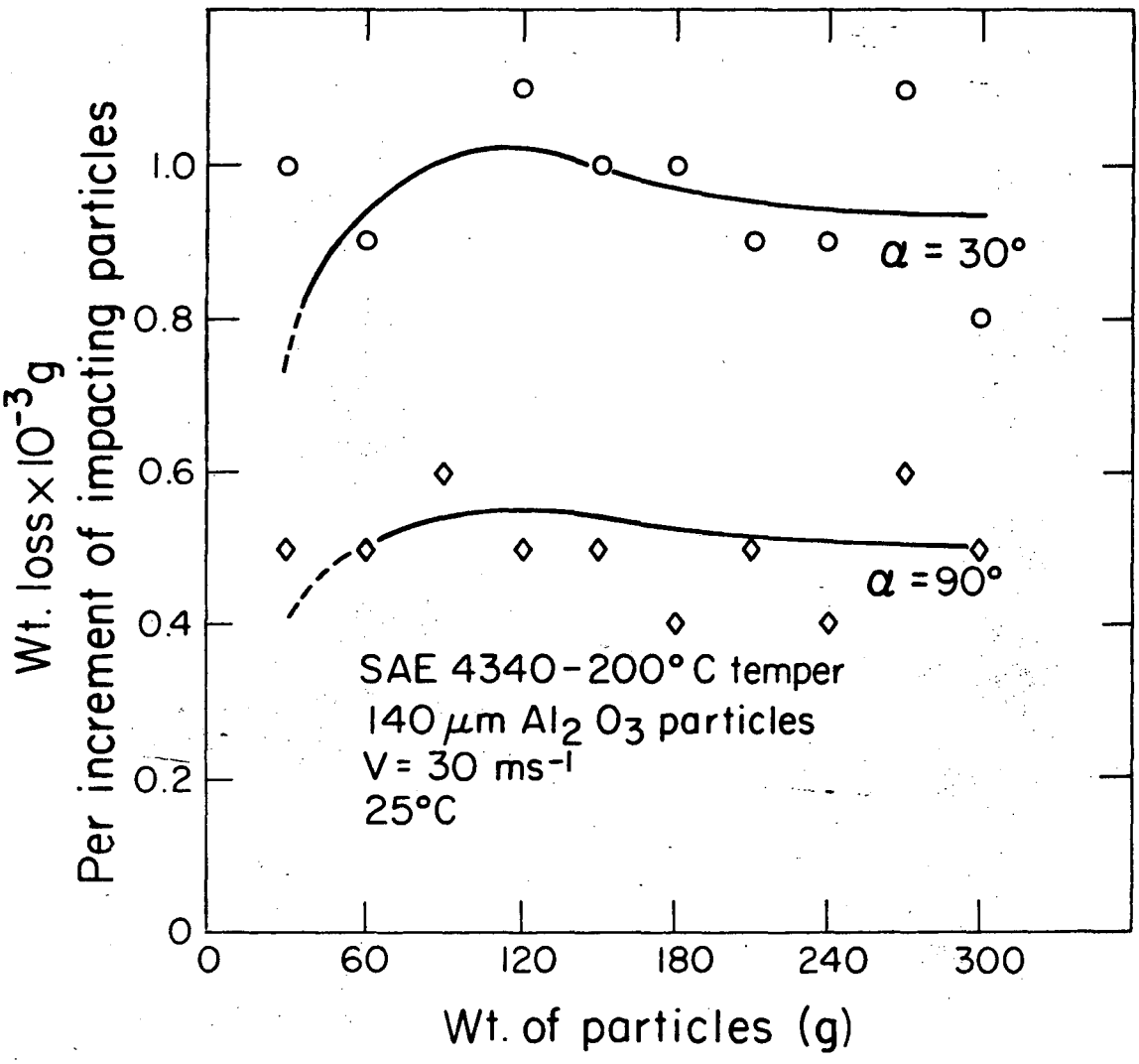

Fig. 15 Erosion of 4340 Steel 200°C temper

XBL8111-12043

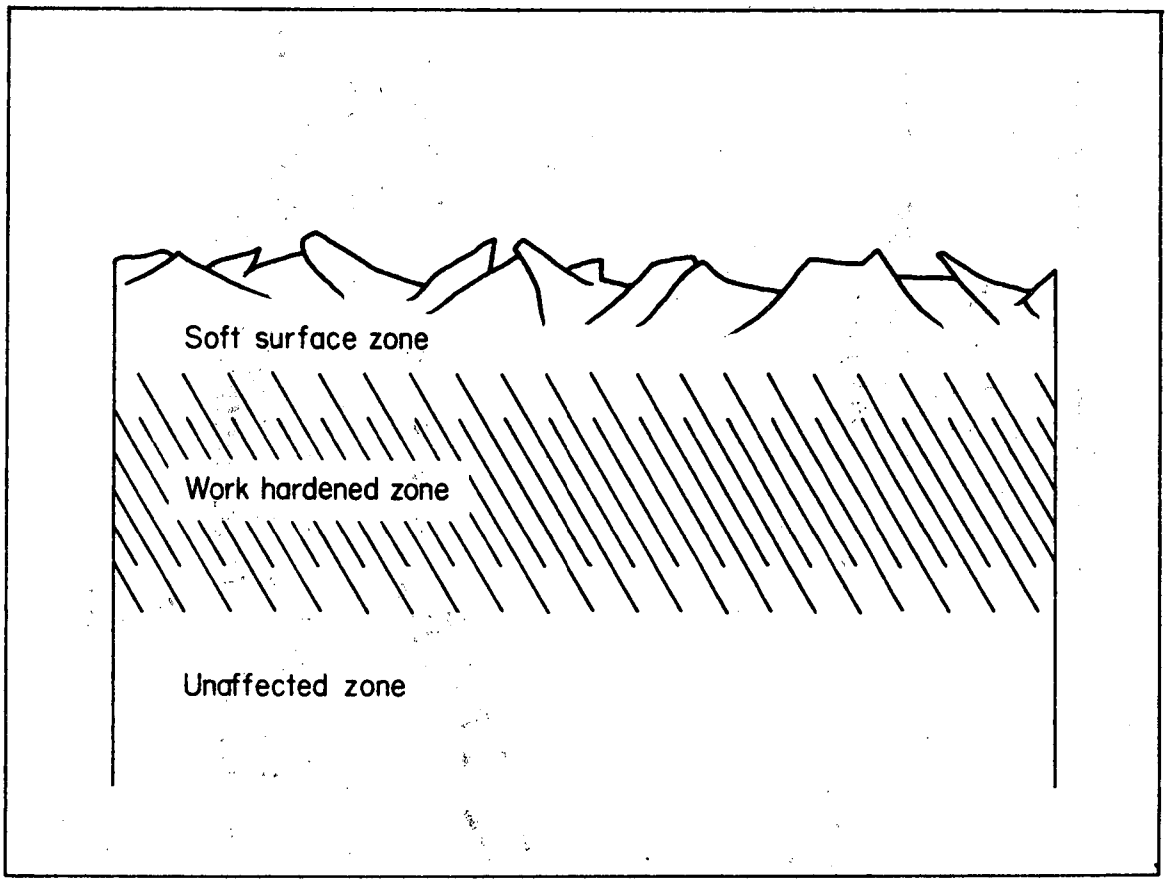

Fig. 16 Illustration of Soft Surface and Work-Hardened Layers with Platelet Formation

XBL 807-10669

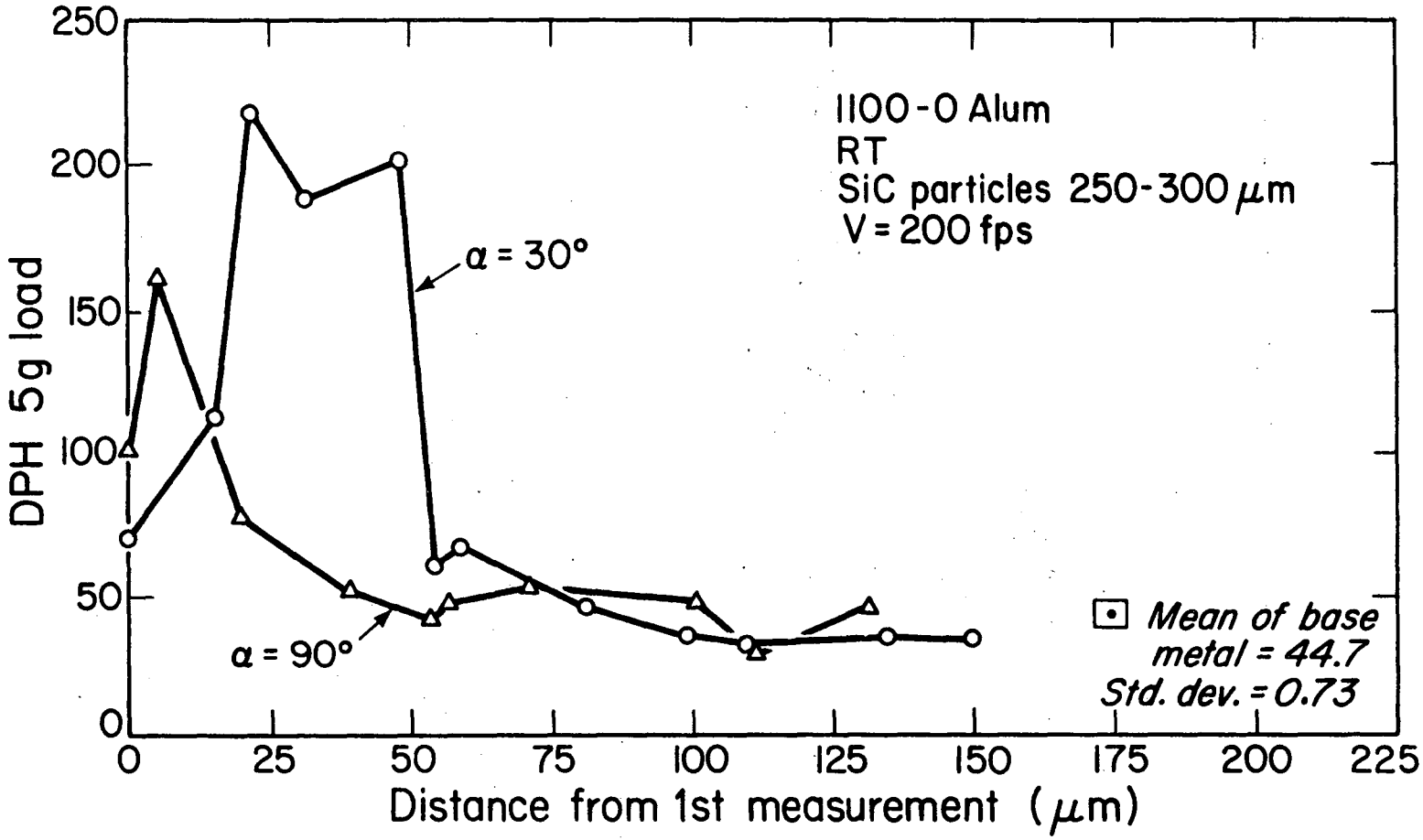

Fig. 17 Micro-Hardness Traverse of Eroded 1100-0 Aluminum ref. [2]

XBL 8011-2236

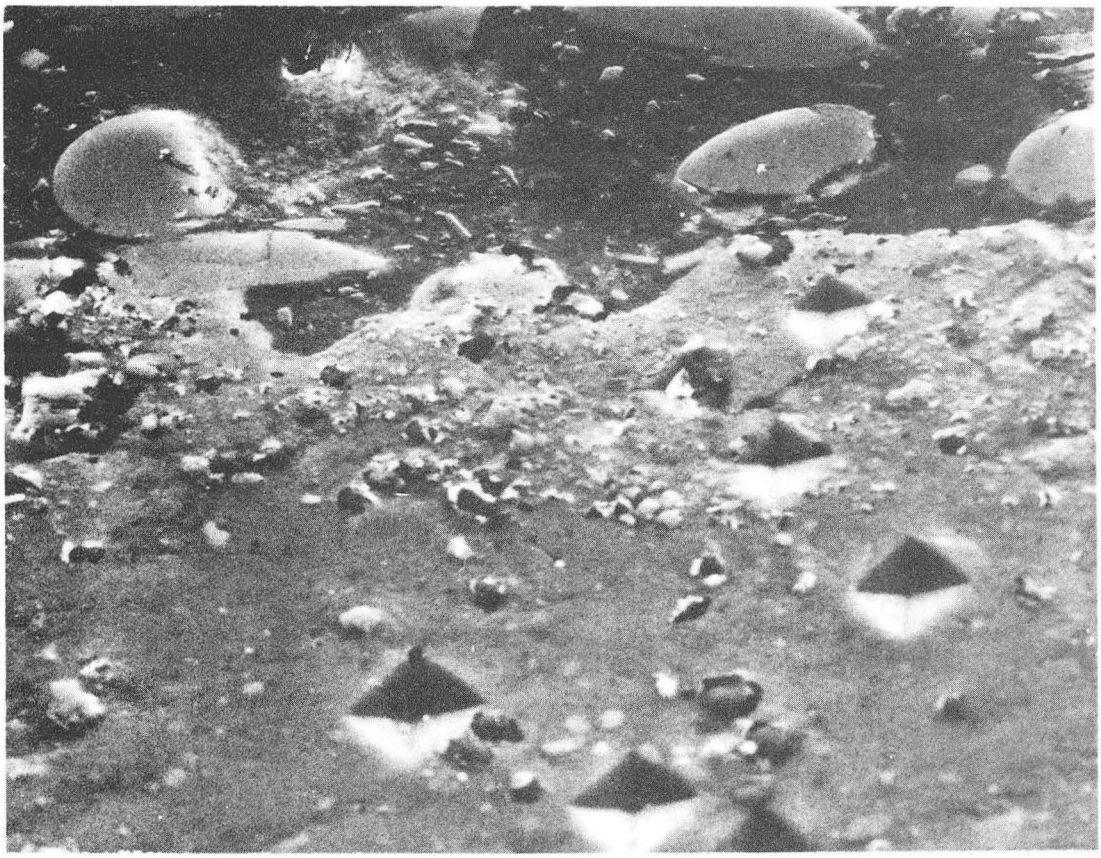

XBB 826-4982

1100-0 Al @ 1000X

10μm

Fig. 18 Cross-Section of 1100-0 Al showing symmetrical micro-hardness indentations

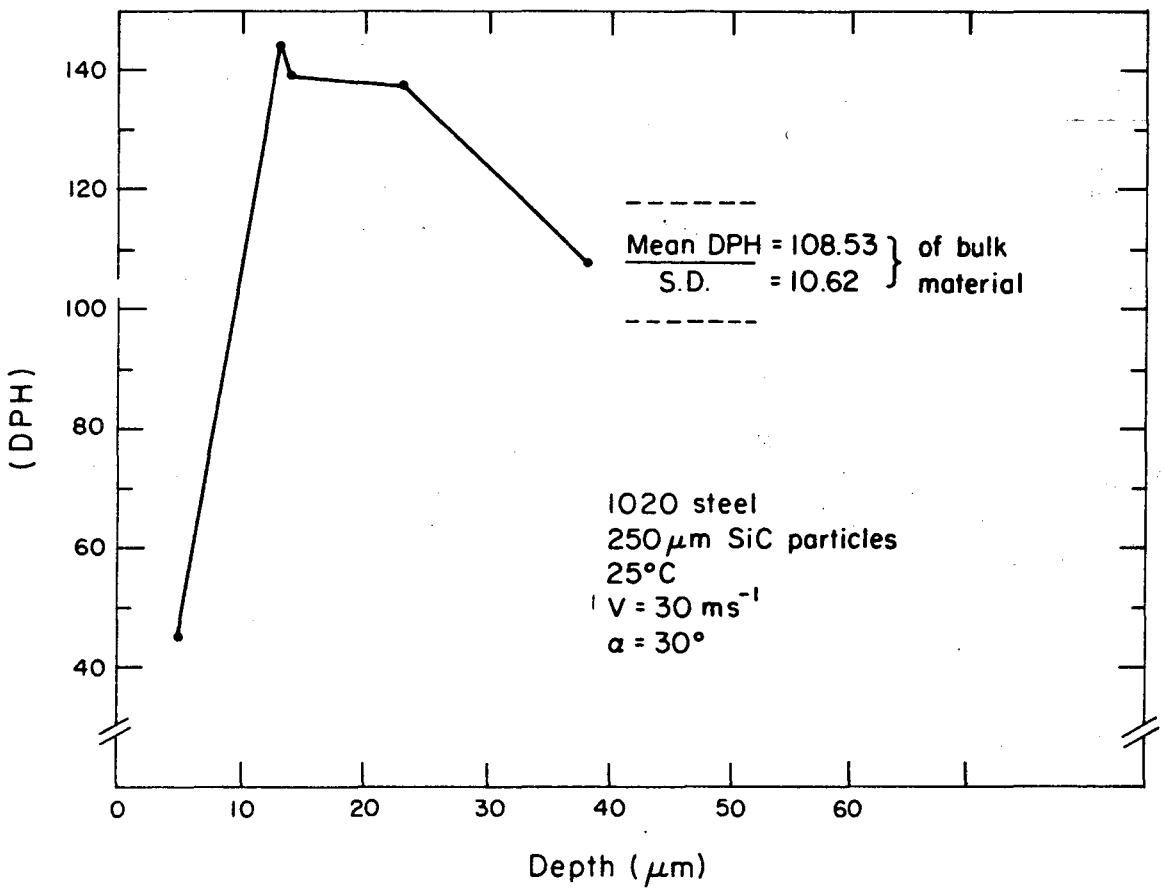

Fig. 19 Micro-Hardness Traverse of eroded 1020 Steel

XBL8111-12038

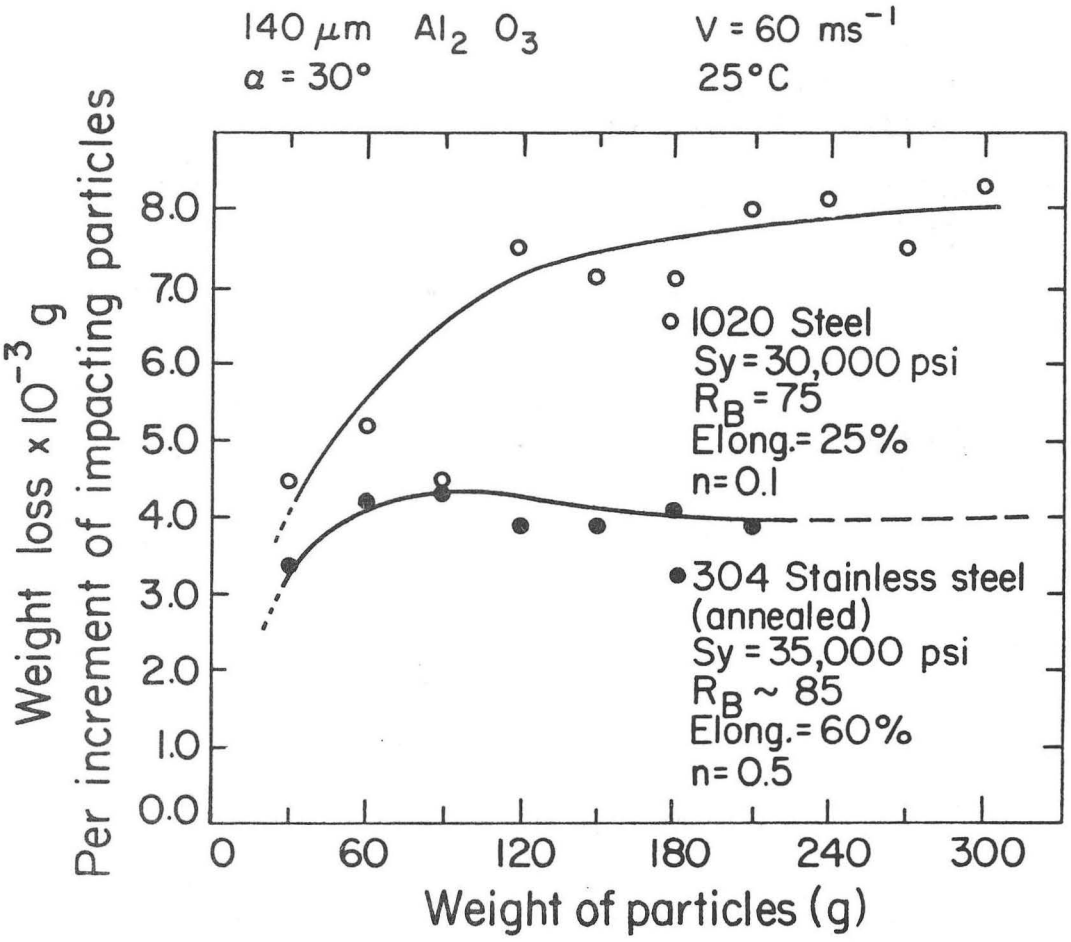

XBL 8110-1395B

Fig. 20 Effect of strain hardening coeff. and elongation on the erosion of 1020 steel and 304 stainless steel

SPHEROIDIZED AISI 1020 STEEL

30°

90°

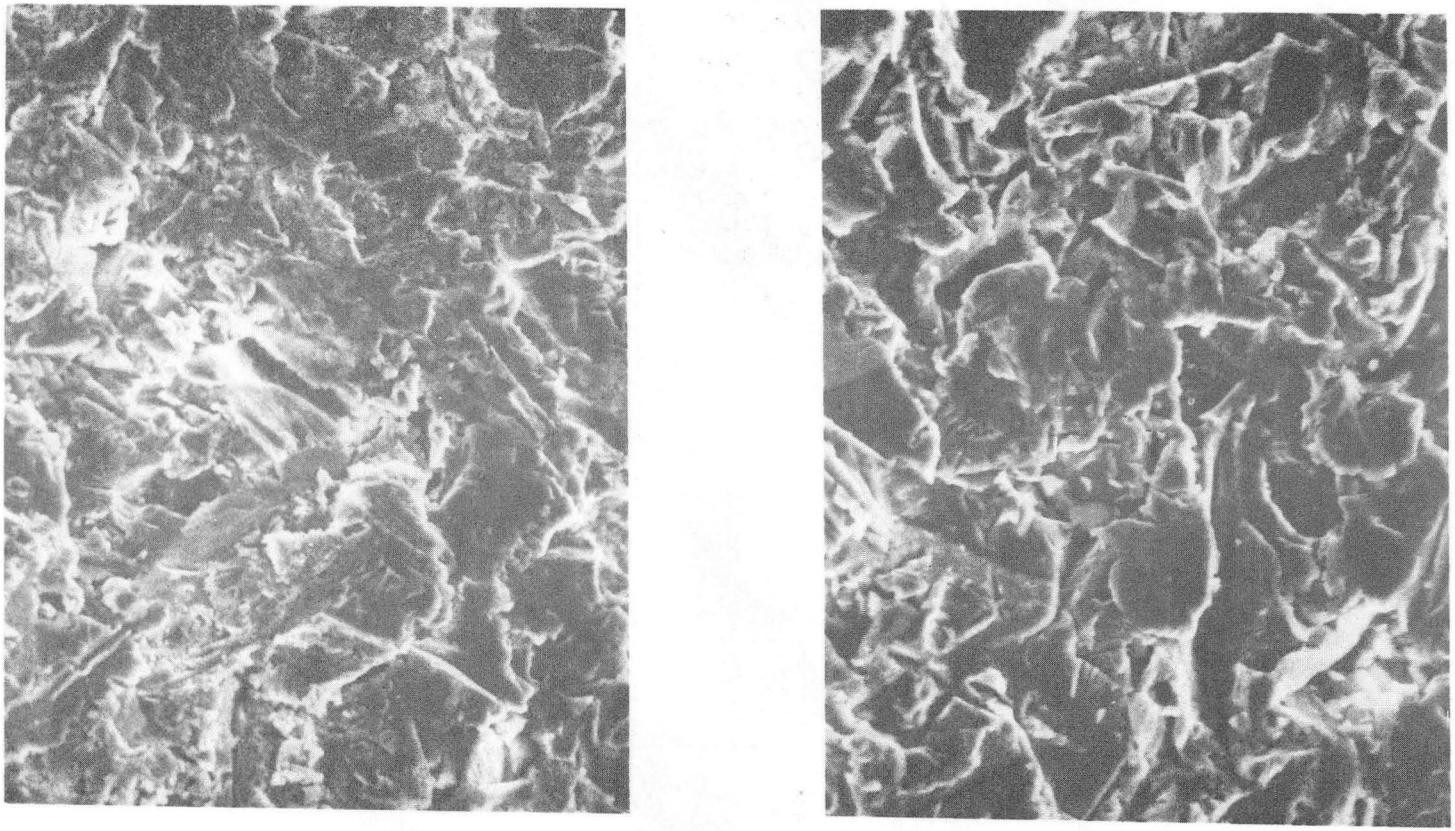

5um

5um

$V = 60\ ms^{-1}$ (200 fps)

140 um Al_2O_3

Fig. 21 Electron Micrograph of Platelets observed on the Eroded surface of a 1020 Steel Specimen at Impingement Angles of 30° and 90°

XBB825-4372

DISTRIBUTION LIST

Wate Bakker
EPRI
Hillview Ave.
Palo Alto, CA 94303

Susan M. Benford
NASA Lewis Research Center
21000 Brookpark Rd.
Cleveland, OH 41135

Mr. R.A. Bradley, Manager
Fossil Energy Materials Program
Oak Ridge National Laboratory
P.O. Box X
Oak Ridge, TN 37830

Richard Brown
Materials Durability Division
College of Engineering
University of Delaware
Newark, DE 19711

Dr. P.T. Carlson, Task Leader
Fossil Energy Materials Program
Oak Ridge National Laboratory
P.O. Box X
Oak Ridge, TN 37830

Mr. J.P. Carr
Department of Energy, Office of Fossil Energy
FE-42, Mailstop 3222-GTN
Washington D.C. 40525

Hans Conrad
Materials Engineering Department
North Carolina State University
Raleigh, NC 27607

Mr. S.J. Dapkunas
Department of Energy, Office of Fossil Energy
Technical Coordination Staff FE-14, Mailstop C-156 GTN
Washington D.C. 40525

DOE Technical Information Center
P.O. Box 62
Oak Ridge, TN 37830

Bill Ellingson
Argonne National Laboratory
9700 South Cass Ave.
Argonne, IL 60439

Mary Ellen Gulden
Solar Turbines International
PO Box 80966
San Diego, CA 92138

Mr. J.M. Hobday
Department of Energy
Morgantown Energy Technology Center
P.O. Box 880
Morgantown, WV 26505

Mr. E.E. Hoffman, Manager
National Materials Programs
Department of Energy
Oak Ridge Operations
P.O. Box E
Oak Ridge, TN 37830

Sven Jansson
Stal-Laval Turbin AB
Finspong S-61220
Sweden

Dr. R.R. Judkins
Fossil Energy Materials Program
Oak Ridge National Laboratory
P.O. Box X
Oak Ridge, TN 37830

Thomas Kosel
University of Notre Dame
Dept. of Metallurgical Engineering & Materials Science
Box E
Notre Dame, IN 46556

Mr. E.L. Long, Jr.
Fossil Energy Materials Program
Oak Ridge National Laboratory
P.O. Box X
Oak Ridge, TN 37830

Norman H. MacMillan
Pennsylvania State University
167 Materials Research Laboratory
University Park, PA 16802

Ken Magee
Bingham-Willamette Co.
2800 N.W. Front Ave.
Portland, OR 97219

Fred Pettit
Dept. of Metallurgy and Materials Engineering
University of Pittsburgh
Pittsburgh, PA 15261

Alberto Sagüés
IMMR – University of Kentucky
763 Anderson Hall
Lexington, KY 40506

Gordon Sargent
University of Notre Dame
Dept. of Metallurgical Engineering & Materials Science
Box E
Notre Dame, IN 46556

Paul Shewmon
Dept. of Metallurgical Engineering
116 W. 19th Ave.
Columbus, OH 43210

John Stringer
EPRI
3412 Hillview Avenue
P.O. Box 10412
Palo Alto, CA 94303

Widen Tabakoff
Dept. of Aerospace Engineering
University of Cincinnati
Cincinnati, OH 45221

Edward Vesely
IITRI
10 West 35th St.
Chicago, IL 60616

J.C. Williams
Dept. of Metallurgy & Materials Science
Carnegie-Mellon University
Schenley Park
Pittsburgh, PA 15213

Ian Wright
Materials Science Division
Battelle Memorial Institute
505 King Ave.
Colombus, OH 43201

TECHNICAL INFORMATION DEPARTMENT
LAWRENCE BERKELEY LABORATORY
UNIVERSITY OF CALIFORNIA
BERKELEY, CALIFORNIA 94720